

# THERMOELECTRIC DEGREES OF FREEDOM DETERMINING THERMOELECTRIC EFFICIENCY

BYUNGKI RYU<sup>†,\*</sup>, JAYWAN CHUNG<sup>†,\*</sup>, AND SUDONG PARK

**ABSTRACT.** Thermal energy can be directly converted to electrical energy as a result of thermoelectric effects. Because this conversion realises clean energy technology, such as waste heat recovery and energy harvesting, substantial efforts have been made to search for thermoelectric materials. Under the belief that the material figure of merit  $zT$  represents the energy conversion efficiencies of thermoelectric devices, various high peak- $zT$  materials have been explored for half a century. However, thermoelectric properties vary greatly with temperature  $T$ , so the single value  $zT$  does not represent device efficiency accurately. Here we show that the efficiency of thermoelectric conversion is completely determined by *three* parameters  $Z_{\text{gen}}$ ,  $\tau$ , and  $\beta$ , which we call the *thermoelectric degrees of freedom*. The  $Z_{\text{gen}}$ , which is an average of material properties, is a generalisation of the traditional figure of merit. The  $\tau$  and  $\beta$ , which reflect the gradients of the material properties, are proportional to escaped heat caused by the Thomson effect and asymmetric Joule heat, respectively. Our finding proposes new directions for achieving high thermoelectric efficiency; increasing one of the thermoelectric degrees of freedom results in higher efficiency. For example, thermoelectric efficiency can be enhanced up to 176% by tuning the thermoelectric degrees of freedom in segmented legs, compared to the best efficiency of single-material legs.

Thermoelectric device can convert heat to electricity by generating electrical voltage across legs operating between a hot side, with temperature  $T_h$ , and cold side, with temperature  $T_c$ . In general, the nonlocality of the thermoelectric equation allows no analytical expression for energy conversion efficiency [1, 2]. However, *if* thermoelectric properties of materials *do not vary with temperature  $T$* , the maximum efficiency of thermoelectric conversion  $\eta_{\text{max}}$  is determined by the dimensionless figure of merit  $zT_m = \frac{\alpha^2}{\rho\kappa}T_m$ , where  $\alpha$  is the Seebeck coefficient,  $\rho$  is the electrical resistivity,  $\kappa$  is the thermal conductivity, and  $T_m$  is the mean of  $T_h$  and  $T_c$ . The  $\eta_{\text{max}}$  for temperature-independent (or constant) material properties is given by the well-known classical formula  $\eta_{\text{max}}^{\text{const}} = \frac{\Delta T}{T_h} \frac{\sqrt{1+zT_m}-1}{\sqrt{1+zT_m+T_c/T_h}}$  where  $\Delta T = T_h - T_c$ . In this classical formula, higher  $zT_m$  implies higher efficiency. With this observation, extensive research on materials has been conducted, improving peak  $zT$  from below 1 to above 2.6 in half a century [3]. Low thermal conductivity and high power factor ( $\alpha^2/\rho$ ) have been achieved by using anharmonic phonon structure, defective structures from atomic scale to micro scale, non-parabolic band structure, electronic structure distortion, and Fermi-level tuning [3–9].

---

(B Ryu, J Chung, and SD Park) ENERGY CONVERSION RESEARCH CENTER, KOREA ELECTROTECHNOLOGY RESEARCH INSTITUTE (KERI), 12, BULMOSANRO 10BEON-GIL, SEONGSAN-GU, CHANGWON, 51543, REPUBLIC OF KOREA

(<sup>†</sup>) B.R. AND J.C. CONTRIBUTED EQUALLY TO THIS WORK

*E-mail addresses:* byungkiryu@keri.re.kr, jchung@keri.re.kr.

*Date:* March 30, 2023.

However, material properties *do* vary greatly with temperature  $T$ , hence a higher peak  $zT$  no longer implies higher device efficiency. In Figure 1, the relationship between the peak  $zT$  and the numerical maximum efficiency divided by the Carnot efficiency  $\eta_{\text{Carnot}} = \frac{\Delta T}{T_h}$  is shown for 276 reported materials under available temperature ranges; see §1 and §2 in Supplementary Information(SI) for details. The  $\eta_{\text{red}}$  can vary by a factor of five between materials even if the peak  $zT$  is the same. The strong correlation among similar materials in Figure 1 is misleading; the correlation exists not because the peak  $zT$  is predictive, but because the  $zT$  ignores the temperature dependencies of the similar materials altogether.

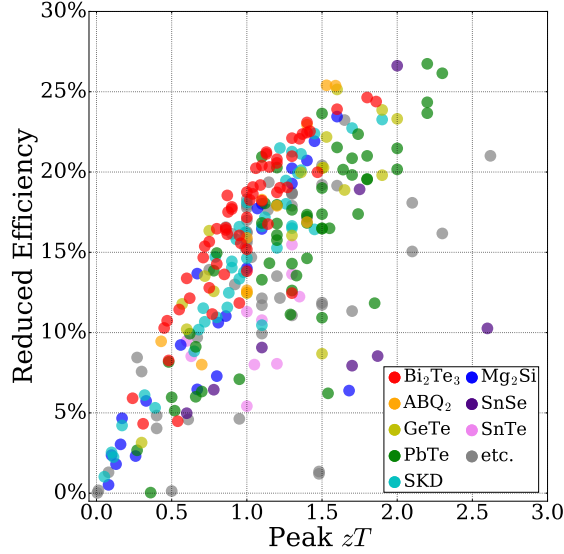


FIGURE 1. Relationship between the reduced efficiency  $\eta_{\text{red}} = \eta_{\text{max}}/\eta_{\text{Carnot}}$  and the peak  $zT$  for 276 reported materials, including Bi<sub>2</sub>Te<sub>3</sub>, PbTe, SnSe, and so on.

To overcome the limitation of the peak  $zT$ , various average parameters have been proposed. Ioffe and Borrero [10–12] suggested an average figure of merit  $z_{\text{av}} = \frac{\langle \alpha \rangle^2}{\langle \rho \kappa \rangle}$ , where the bracket  $\langle \cdot \rangle$  indicates averaging over  $T$ , from *constant heat-current approximation*. However, the average  $z$  or  $Z$  does not predict efficiency accurately, due to a disregard for the Thomson effect and the non-uniformity of Joule heat, as well as poor approximation of the temperature distribution [12–16]. Snyder and Snyder [17] defined *device*  $ZT$  in terms of  $\eta_{\text{max}}$ :  $(ZT)_{\text{dev}} := \left( \frac{T_h - T_c(1 - \eta_{\text{max}})}{T_h(1 - \eta_{\text{max}}) - T_c} \right)^2 - 1$ . However, while the  $(ZT)_{\text{dev}}$  satisfies the classical efficiency formula, it gives no method to compute  $\eta_{\text{max}}$ . Kim et al. [18–20] suggested an efficiency formula using *engineering*  $ZT$  and Thomson correction parameters. Their efficiency formula accounts for strong temperature dependence of material properties; for example, SnSe has the peak  $zT$  value of 2.6 at 923 K while the  $zT$  vanishes near the room temperature [3]. However, it still contains about 9% error for SnSe due to the *linear approximation of temperature*. One may consider the compatibility factor  $s = \frac{\sqrt{1+zT}-1}{\alpha T}$ , suggested by Snyder and Ursell [21]. As a function of  $T$ , the uniformity of  $s(T)$  may indicate high efficiency. However, the  $s$  is not a figure of merit; higher  $s$  does not imply

higher efficiency, while higher  $zT$  partially does. In summary, no *single* value has been successful in predicting thermoelectric conversion efficiency as a figure of merit.

**Main Result.** In this paper, we show that thermoelectric conversion efficiency  $\eta$  is *completely determined* by three independent parameters  $Z_{\text{gen}}$ ,  $\tau$ , and  $\beta$ . Because they determine the performance of thermoelectric devices, we call them the *thermoelectric degrees of freedom*. The  $Z_{\text{gen}}$  is an average of material properties, and it generalises the traditional figure of merit. The additional degrees of freedom  $\tau$  and  $\beta$ , which reflect the gradients of the material properties, are proportional to the escaped heat caused by the Thomson effect and the asymmetric Joule heat respectively. We omit exact involved definitions of  $Z_{\text{gen}}$ ,  $\tau$ , and  $\beta$  here because there is a simple but accurate approximation formula in equation (2) for them; for the exact definitions, see §5 and §8 in SI. The schematic diagram in Figure 2 shows the relationship between material properties and the thermoelectric degrees of freedom, where the temperature-dependent material properties are decomposed into averaged and gradient parts, and they are represented by the degrees of freedom. Efficiency is a function of the thermoelectric degrees of freedom when the

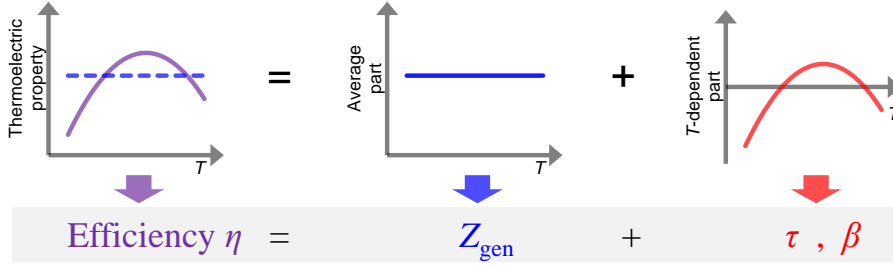


FIGURE 2. A schematic diagram explaining the relationship between temperature-dependent material properties and thermoelectric degrees of freedom  $Z_{\text{gen}}$ ,  $\tau$ , and  $\beta$ . The  $Z_{\text{gen}}$  represents the averaged part of material properties, while the  $\tau$  and  $\beta$  represent the gradient parts of them.

electric current  $I$  is given:  $\eta = \eta(Z_{\text{gen}}, \tau, \beta | I)$ . Furthermore, each degree of freedom is a figure of merit because  $\eta(Z_{\text{gen}}, \tau, \beta)$  is monotone increasing in each variable; see §9 in SI. The maximum efficiency can be simply approximated by the following formula:

$$(1) \quad \eta_{\text{max}} = \eta_{\text{max}}(Z_{\text{gen}}, \tau, \beta | I = I_{\text{opt}}) \approx \eta_{\text{max}}^{\text{gen}}(Z_{\text{gen}}, \tau, \beta) := \frac{\Delta T}{T'_h} \frac{\sqrt{1 + Z_{\text{gen}} T'_m} - 1}{\sqrt{1 + Z_{\text{gen}} T'_m + \frac{T'_c}{T'_h}}},$$

where  $I_{\text{opt}}$  is the optimal current giving the maximum efficiency,  $T'_h = T_h - \tau \Delta T$ ,  $T'_c = T_c - (\tau + \beta) \Delta T$ , and  $T'_m = (T'_h + T'_c)/2$ . The general formula  $\eta_{\text{max}}^{\text{gen}}$  is identical to the classical formula  $\eta_{\text{max}}^{\text{const}}$  except for the modification of temperature parameters. While exact computation of the  $Z_{\text{gen}}$ ,  $\tau$ , and  $\beta$  requires temperature distribution inside the device, they can be easily estimated using *one-shot approximation* assuming constant heat current and linear thermoelectric properties; see §10 in SI. The one-shot approximation

gives

(2)

$$Z_{\text{gen}} \approx Z_{\text{gen}}^{(0)} := \frac{\left(\int_{T_c}^{T_h} \alpha dT\right)^2}{\Delta T \int_{T_c}^{T_h} \rho\kappa dT}, \quad \tau \approx \tau_{\text{lin}}^{(0)} := -\frac{1}{3} \frac{\alpha_h - \alpha_c}{\alpha_h + \alpha_c}, \quad \beta \approx \beta_{\text{lin}}^{(0)} := \frac{1}{3} \frac{(\rho\kappa)_h - (\rho\kappa)_c}{(\rho\kappa)_h + (\rho\kappa)_c},$$

where the subscripts  $h$  and  $c$  indicate the material properties evaluated at  $T_h$  and  $T_c$  respectively. When the material properties are temperature-independent, the above formulas,  $\eta_{\text{max}}^{\text{gen}}$ ,  $Z_{\text{gen}}^{(0)}$ ,  $\tau_{\text{lin}}^{(0)}$  and  $\beta_{\text{lin}}^{(0)}$  in equation (1) and (2), become  $\eta_{\text{max}}^{\text{const}}$  and the traditional figure of merit,  $Z_{\text{gen}} = z$ , with vanishing  $\tau$  and  $\beta$ . The simple formula in equation (1) with equation (2) predicts maximum efficiency with high accuracy; see Figure 3. Besides

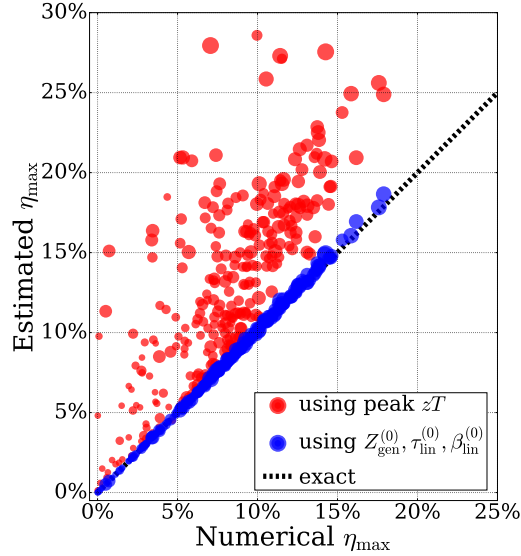


FIGURE 3. Comparison of two estimation methods for maximum efficiency; one uses the classical formula  $\eta_{\text{max}}^{\text{const}}$  with peak  $zT$  (red circle), and the other uses our efficiency formula  $\eta_{\text{max}}^{\text{gen}}$  in equation (1), with the *one-shot approximation* of the thermoelectric degrees of freedom in equation (2) (blue circle). The estimated values are compared with the exact, numerical maximum efficiency for 276 materials under available temperature range. The marker size is proportional to the peak  $zT$ .

predicting efficiency, the thermoelectric degrees of freedom suggest new directions for improving it. Since each of  $Z_{\text{gen}}$ ,  $\tau$ , and  $\beta$  is a figure of merit, by increasing one of them, we can improve efficiency; see Figure 4(a),(b). Segmenting a leg with different materials is a way of tuning the degrees of freedom and increasing efficiency. In this way, efficiency can be enhanced up to 170% compared to single-material legs; see Figure 4(c).

In the following sections, we sketch derivation of the thermoelectric degrees of freedom, and give more practical applications of them. Full derivation can be found in SI.

**Temperature Distribution.** The thermoelectric effect is expressed in terms of electric current density  $J$  and heat current density  $J^Q$ :  $J = \sigma(E - \alpha\nabla T)$  and  $J^Q = \alpha T J - \kappa\nabla T$  where  $E$  is the electric field. Applying the charge and energy conservation laws to  $J$

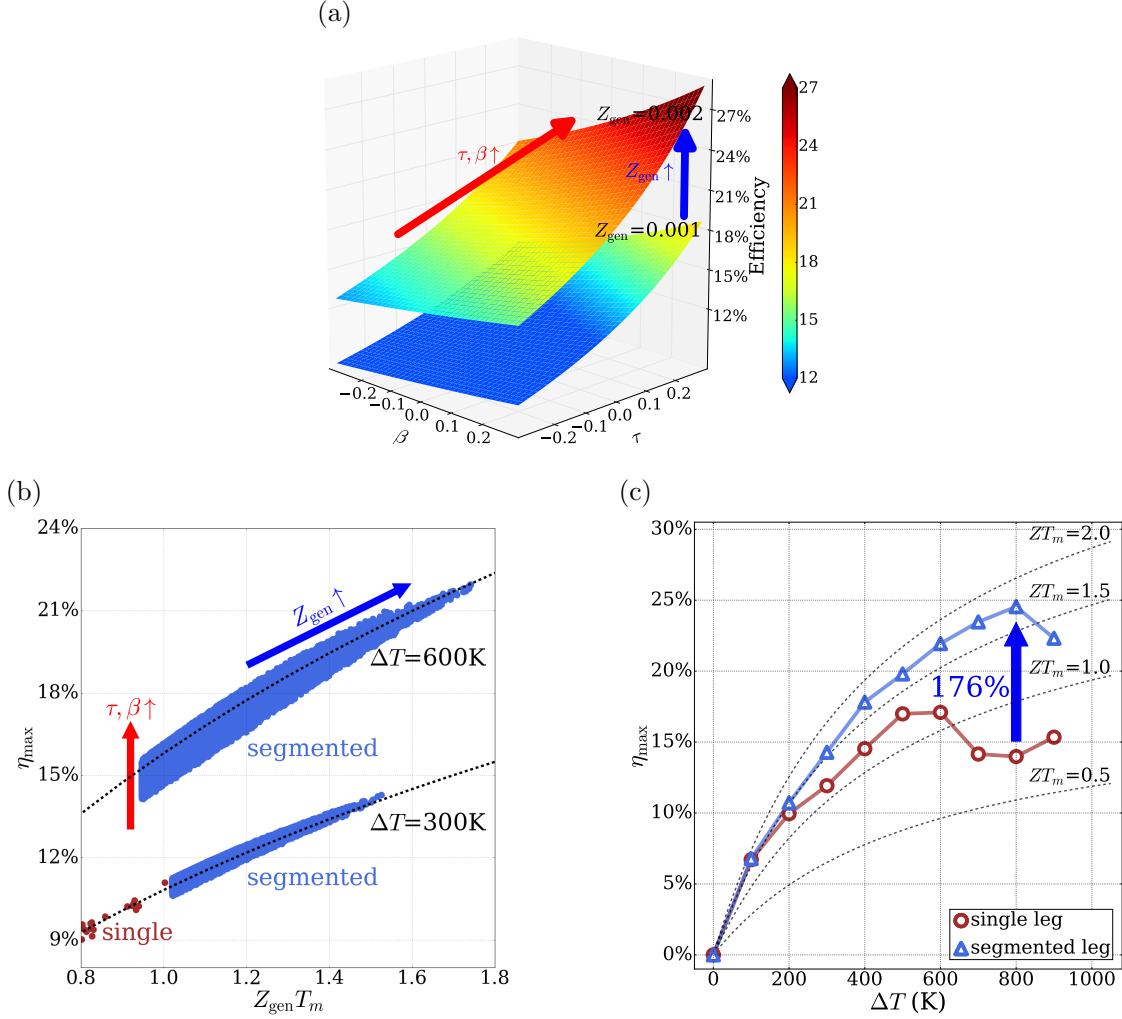


FIGURE 4. (a) Efficiency surface  $\eta_{\max}^{\text{gen}}(Z_{\text{gen}}, \beta, \tau)$  in equation (1) is drawn for  $Z_{\text{gen}} = 0.002K^{-1}$  and  $0.001K^{-1}$ , for fixed  $T_h = 900K$  and  $T_c = 300K$ . Improving one of three thermoelectric degrees of freedom  $Z_{\text{gen}}, \tau, \beta$  increases the efficiency. (b) Numerical maximum efficiencies for single-material legs (brown circle) and segmented legs (blue circle) for  $T_c = 300K$  and  $\Delta T = 300K$  or  $600K$ . For the segmented legs, we consider  $18^5 = 1,889,568$  configurations up to 5-stage segmentation consisting of 18 candidate materials; for material information, see §1 in SI. Here only the top 100,000 configurations are shown. Notice that the segmentation can control the thermoelectric degrees of freedom. (c) Maximum possible efficiencies among single-material legs (brown open circle) and segmented legs (blue open triangle) for  $T_c = 300K$  and given  $\Delta T$ . The leg segmentation can enhance the maximum efficiency up to 176%.

and  $J^Q$ , we can obtain the thermoelectric differential equation of temperature  $T$  in a

one-dimensional thermoelectric leg [1, 2]:

$$(3) \quad \frac{d}{dx} \left( \kappa \frac{dT}{dx} \right) + \rho J^2 - T \frac{d\alpha}{dT} \frac{dT}{dx} J = 0$$

where  $x$  is the spatial coordinate inside the leg. The left-hand side of equation (3) is composed of thermal diffusion, Joule heat generation, and Thomson heat generation. Here, we obtain an *integral* equation for  $T = T(x)$  by integrating the equation (3) twice. The integral equation is of the form  $T = \varphi[T]$  where  $\varphi$  is an integral operator; see §7 in SI. With this relation, the exact  $T$  can be obtained via fixed-point iteration  $T_{n+1} = \varphi[T_n]$  [22]. An approximate  $T$  can be obtained from  $T = \varphi[T^{(0)}]$ , where  $T^{(0)}$  is the solution of equation (3) when  $J = 0$ . Once the temperature distribution  $T$  is found, the thermoelectric performance and efficiency can be easily computed.

**Electrical Power.** To compute open-circuit voltage  $V$ , electrical resistance  $R$ , and thermal resistance  $1/K$ , it is natural to integrate the material properties on the spatial coordinate  $x$  inside the leg (not on  $T$ ) because the electric current and the heat current flow through the leg. Hence we define average parameters of material properties as  $\bar{\alpha} := \frac{V}{\Delta T} = \int \alpha \frac{dT}{dx} dx$ ,  $\bar{\rho} := \frac{A}{L} R = \frac{1}{L} \int \rho dx$ , and  $\frac{1}{\bar{\kappa}} := \frac{A}{L} \frac{1}{K} = \frac{1}{L} \int \frac{1}{\kappa} dx$ , where  $L$  and  $A$  are the length and area of the leg. The electric current is determined as  $I = \frac{V}{R(1+\gamma)}$ , where  $\gamma$  is the ratio of the load resistance  $R_L$  outside the device to the resistance of the thermoelectric leg  $R$ . The power delivered to the load is  $P = I^2 R_L = I(V - IR) = \frac{\bar{\alpha}^2 \Delta T^2}{\bar{\rho}} \frac{\gamma}{L/A (1+\gamma)^2}$ , which is maximised near  $\gamma = 1$ . Using the average properties, we define the *general device power factor* as  $PF_{\text{gen}} := \frac{\bar{\alpha}^2}{\bar{\rho}}$  and the *general device figure of merit* as  $Z_{\text{gen}} = \frac{\bar{\alpha}^2}{RK} = \frac{\bar{\alpha}^2}{\bar{\rho}\bar{\kappa}}$ .

**Heat Current.** If the material properties do not depend on  $T$ , the heat current of the hot and cold sides are determined by the average parameters:  $\overline{Q}_h = K\Delta T + I\bar{\alpha}T_h - \frac{1}{2}I^2R$  and  $\overline{Q}_c = K\Delta T + I\bar{\alpha}T_c + \frac{1}{2}I^2R$ . The power delivered outside is  $P = \overline{Q}_h - \overline{Q}_c$ . If the material properties *depend on*  $T$ , the heat currents change to other values  $Q_h$  and  $Q_c$  but their difference remains unchanged, indicating that the power remains unchanged as well:  $P = Q_h - Q_c = \overline{Q}_h - \overline{Q}_c$ . Thus, we have a relation  $P = Q_h - Q_c = (\overline{Q}_h - B) - (\overline{Q}_c - B)$ , implying that both of the heat currents are shifted by the same *backward heat current*  $B$ . We prove that  $B$  is determined from the gradient parameters  $\tau$  and  $\beta$ :  $B = (I\bar{\alpha}\Delta T)\tau + (\frac{1}{2}I^2R)\beta$ ; see §8 in SI. Hence the heat currents at the boundaries are determined as

$$(4) \quad \begin{aligned} Q_h &= K\Delta T + I\bar{\alpha}(T_h - \tau\Delta T) - \frac{1}{2}I^2R(1 + \beta), \\ Q_c &= K\Delta T + I\bar{\alpha}(T_c - \tau\Delta T) + \frac{1}{2}I^2R(1 - \beta). \end{aligned}$$

Note that the heat currents are changed by the effective Thomson heat flow  $(-I\bar{\alpha}\Delta T)\tau$  and the asymmetric Joule heat escape  $(-\frac{1}{2}I^2R)\beta$  due to the temperature dependency.

**Efficiency.** Thermoelectric efficiency is defined as  $\eta := \frac{Q_h - Q_c}{Q_h}$ . From equation (4), we can verify that the dimensionless heat current,  $\frac{Q_h}{K\Delta T}$  and  $\frac{Q_c}{K\Delta T}$ , and the efficiency are determined by five parameters  $Z_{\text{gen}}$ ,  $\tau$ ,  $\beta$ ,  $\Delta T$ , and  $\gamma$ . Furthermore, for fixed  $\Delta T$  and  $\gamma$ , the efficiency is monotone increasing with respect to  $Z_{\text{gen}}$ ,  $\tau$ , and  $\beta$  (see Figure 4(a)), which implies that each of the degrees of freedom  $Z_{\text{gen}}$ ,  $\tau$ , and  $\beta$  is a figure of merit.

Although the degrees of freedom depend on  $\gamma$ , the dependency is negligible near the  $\gamma_{\max}$  where the maximum efficiency occurs, because the temperature distribution hardly changes for  $\gamma$  in most thermoelectric materials. Hence we may assume that the degrees of freedom in  $\eta(Z_{\text{gen}}, \tau, \beta|\gamma)$  are fixed, independent values and maximise the  $\eta$  only for  $\gamma$  to find an approximate maximum efficiency. In this way we have the simple approximate formula  $\eta_{\max}^{\text{gen}}$  in equation (1) when  $\gamma$  is near the  $\gamma_{\max}^{\text{gen}} := \sqrt{1 + Z_{\text{gen}} T_m}$ ; see §9 in SI.

**One-Shot Approximation.** The thermoelectric degrees of freedom can be directly estimated from the material properties using formula equation (2) for  $Z_{\text{gen}}^{(0)}$ ,  $\tau_{\text{lin}}^{(0)}$  and  $\beta_{\text{lin}}^{(0)}$ . To derive the formula, we assume the temperature distribution inside the leg to be  $T^{(0)}$ , which is the temperature distribution for the  $J = 0$  case (i.e.,  $-\kappa \frac{dT}{dx} = \text{const.}$ ); the superscript (0) means we use the  $J = 0$  case. Furthermore, we assume the material properties  $\alpha$  and  $\rho \times \kappa$  are linear with respect to  $T$ ; the subscripts in  $\tau_{\text{lin}}^{(0)}$  and  $\beta_{\text{lin}}^{(0)}$  emphasize this linearity. We then have the formula equation (2); see §10 and §11 in SI for its derivation and accuracy. The general device power factor can be similarly estimated as  $PF_{\text{gen}}^{(0)} = Z_{\text{gen}}^{(0)} \int \kappa dT$ . This *one-shot approximation* clarifies the relationship between the material properties and the thermoelectric efficiency; for example, because  $\tau \approx -\frac{1}{3} \frac{\alpha_h - \alpha_c}{\alpha_h + \alpha_c}$ , the  $\tau$  (and the efficiency) can be enhanced if the  $\alpha(T)$  declines more rapidly on  $T$ . The one-shot approximation is accurate even for segmented devices. The performance of two-stage segmented device composed of SnSe and BiSbTe at  $\Delta T = 660K - 320K$  is well described by  $\eta_{\max}(Z_{\text{gen}}^{(0)}, \tau^{(0)}, \beta^{(0)}|\gamma)$  over the whole  $\gamma$  range for power generation; see §10 and Figure S5 in SI. Moreover, in high-performance materials, higher  $Z_{\text{gen}}^{(0)}$  usually implies higher thermoelectric efficiency even for segmented materials. Hence the top-ranked devices in order of their efficiency can be screened out quickly by using  $Z_{\text{gen}}^{(0)}$  only. As an example, the efficiencies of 5-stage segmented devices comprised of 18 candidate materials are computed. Of nearly two million combinations of the segmented legs ( $18^5 = 1,889,568$ ), a top 1% high- $Z_{\text{gen}}^{(0)}$  device is also a top 1% high-efficiency device with 82% probability; see §12 in SI.

**Application.** Our finding gives new direction for evaluation of thermoelectric materials and the design of thermoelectric devices, beyond  $zT$ . When  $Z_{\text{gen}}$  is modest, higher  $\tau$  and  $\beta$  may increase the thermoelectric performance. For example, while the single crystalline SnSe has the highest peak  $zT$  of 2.6 [3], Bi<sub>2</sub>Te<sub>3</sub>-based material has higher maximum efficiency. This is because Bi<sub>2</sub>Te<sub>3</sub> has a much higher  $\tau$  than SnSe, due to its temperature-dependent material properties; see §13 in SI for details.

Modulation of the thermoelectric degrees of freedom in functionally graded or segmented devices results in enhanced designs. For example, we can design high-efficiency graded devices using Bi<sub>2</sub>Te<sub>3</sub> by finding the optimal carrier concentration of each segmented region; see §14 in SI. We can also explore the efficiency space of segmented devices to check the current status and the limit of thermoelectric conversion. We achieve a theoretical maximum efficiency  $\eta_{\max}$  of 22.4% at  $\Delta T = 600K$  using leg segmentation; see Figure 4(c). Using the segmented legs, the efficiency is highly enhanced, up to 176%, when  $\Delta T > 600K$ .

**Conclusion.** Three degrees of freedom in thermoelectrics,  $Z_{\text{gen}}$ ,  $\tau$ , and  $\beta$ , completely determine thermoelectric conversion efficiency, and they can be easily estimated from

material properties. Each degree of freedom is a figure of merit, so improving one is a new way to increase efficiency. Modulating the thermoelectric degrees of freedom in segmented materials and legs, the efficiency can be enhanced up to 176% compared to single-material devices.

#### ACKNOWLEDGEMENT

This work was supported by Korea Electrotechnology Research Institute (KERI) Primary research program through the National Research Council of Science and Technology (NST) funded by the Ministry of Science and ICT (MSIT) of the Republic of Korea (No. 18-12-N0101-34) and partially supported by the Korea Institute of Energy Technology Evaluation and Planning (KETEP) and the Ministry of Trade, Industry and Energy (MOTIE) of the Republic of Korea (No. 20162000000910 and No. 20172010000830).

#### CONTRIBUTIONS

† B.R. and J.C. contributed equally to this work. B.R. and S.D.P. designed the project. S.D.P. helped supervise the the project. B.R. and J.C. developed the theoretical formalism, designed the computational framework, performed the calculations, analysed the results. All authors, B.R., J.C. and S.D.P. discussed the results. B.R. and J.C. wrote the paper.

#### COMPETING INTERESTS

The authors declare no competing financial interests.

#### CORRESPONDING AUTHOR

Correspondence to Byungki Ryu (byungkiryu@keri.re.kr) or Jaywan Chung. (jchung@keri.re.kr).

#### METHODS

**Thermoelectric properties data.** Three thermoelectric properties (TEPs), Seebeck coefficient, electrical resistivity, and thermal conductivity, of 276 materials are gathered and digitised from 264 literatures. In each reference, one sample, having the highest  $zT$  value, is chosen for each type of material. If there are both  $p$ - and  $n$ -type materials, we sampled two TEP datasets. The constructed thermoelectric property database consists of various material groups based on  $\text{Bi}_2\text{Te}_3$ ,  $\text{PbTe}$ ,  $\text{SnSe}$ ,  $\text{GeTe}$ ,  $\text{AgSbTe}_2$ ,  $\text{Mg}_2\text{Si}$ ,  $\text{Si}_{1-x}\text{Ge}_x$ , half-Heusler, skutterudite (SKD), and so on. The available temperature range of materials is determined from the available data range for TEPs, and linear interpolation is used to evaluate TEPs at arbitrary temperatures not given in the literatures.

**Thermoelectric efficiency.** Using the temperature-dependent material properties, the thermoelectric efficiencies are calculated. To describe the ideal maximum efficiency of a thermoelectric material, we assume a one-dimensional uni-leg, ignoring heat transfer by convection and radiation, as well as the non-ideal electrical and thermal losses occurred outside the material. The temperature distribution  $T(x)$  is determined by solving the differential equation modelling the thermoelectric effect with Dirichlet boundary conditions where, at the end points, the temperature is fixed by the available temperature range. The thermoelectric performance is calculated as a function of electric current density  $J$ ,



given as  $\eta(J) = \frac{J \left( \int_{T_c}^{T_h} \alpha dT - J \int_{T_c}^{T_h} \rho dx \right)}{-\left( \kappa \frac{dT}{dx} \right)_h + J \alpha_h T_h}$ . The maximum numerical efficiency  $\eta_{\max}$  is searched so that the relation  $\eta(J) \leq \eta_{\max}$  holds.

## REFERENCES

- [1] Goupil, C. *Continuum theory and modeling of thermoelectric elements* (John Wiley & Sons, 2015).
- [2] Chung, J. & Ryu, B. Nonlocal problems arising in thermoelectrics. *Mathematical Problems in Engineering* **2014** (2014).
- [3] Zhao, L.-D. *et al.* Ultralow thermal conductivity and high thermoelectric figure of merit in SnSe crystals. *Nature* **508**, 373–377 (2014).
- [4] Biswas, K. *et al.* High-performance bulk thermoelectrics with all-scale hierarchical architectures. *Nature* **489**, 414–418 (2012).
- [5] Kim, S. I. *et al.* Dense dislocation arrays embedded in grain boundaries for high-performance bulk thermoelectrics. *Science* **348**, 109–114 (2015).
- [6] Snyder, G. J. & Toberer, E. S. Complex thermoelectric materials. *Nature Materials* **7**, 105–114 (2008).
- [7] Heremans, J. P. *et al.* Enhancement of thermoelectric efficiency in PbTe by distortion of the electronic density of states. *Science* **321**, 554–557 (2008).
- [8] Pei, Y. *et al.* Convergence of electronic bands for high performance bulk thermoelectrics. *Nature* **473**, 66–69 (2011).
- [9] Liu, W. *et al.* Convergence of conduction bands as a means of enhancing thermoelectric performance of  $n$ -type  $\text{Mg}_2\text{Si}_{1-x}\text{Sn}_x$  solid solutions. *Physical Review Letters* **108**, 166601 (2012).
- [10] Ioffe, A. F. *Semiconductor thermoelements and thermoelectric cooling* (Infosearch, London, 1957).
- [11] Borrego Larralde, J. M. *Optimum impurity concentration in semiconductor thermoelements*. Ph.D. thesis, Massachusetts Institute of Technology (1961).
- [12] Sherman, B., Heikes, R. & Ure Jr, R. Calculation of efficiency of thermoelectric devices. *Journal of Applied Physics* **31**, 1–16 (1960).
- [13] Sunderland, J. E. & Burak, N. T. The influence of the Thomson effect on the performance of a thermoelectric power generator. *Solid-State Electronics* **7**, 465–471 (1964).
- [14] Wee, D. Analysis of thermoelectric energy conversion efficiency with linear and nonlinear temperature dependence in material properties. *Energy Conversion and Management* **52**, 3383–3390 (2011).
- [15] Sandoz-Rosado, E. J., Weinstein, S. J. & Stevens, R. J. On the Thomson effect in thermoelectric power devices. *International Journal of Thermal Sciences* **66**, 1–7 (2013).
- [16] Ju, C., Dui, G., Zheng, H. H. & Xin, L. Revisiting the temperature dependence in material properties and performance of thermoelectric materials. *Energy* **124**, 249–257 (2017).
- [17] Snyder, G. J. & Snyder, A. H. Figure of merit  $ZT$  of a thermoelectric device defined from materials properties. *Energy & Environmental Science* **10**, 2280–2283 (2017).
- [18] Kim, H. S., Liu, W., Chen, G., Chu, C.-W. & Ren, Z. Relationship between thermoelectric figure of merit and energy conversion efficiency. *Proceedings of the National Academy of Sciences* **112**, 8205–8210 (2015).
- [19] Kim, H. S., Liu, W. & Ren, Z. Efficiency and output power of thermoelectric module by taking into account corrected Joule and Thomson heat. *Journal of Applied Physics* **118**, 115103 (2015).
- [20] Kim, H. S., Liu, W. & Ren, Z. The bridge between the materials and devices of thermoelectric power generators. *Energy & Environmental Science* **10**, 69–85 (2017).
- [21] Snyder, G. J. & Ursell, T. S. Thermoelectric efficiency and compatibility. *Physical Review Letters* **91**, 148301 (2003).
- [22] Burden, R. L. & Faires, J. D. *Numerical analysis* (Brooks/Cole, Cengage Learning, 2010), 9th edn.

**SUPPLEMENTARY INFORMATION FOR  
“THERMOELECTRIC DEGREES OF FREEDOM DETERMINING  
THERMOELECTRIC EFFICIENCY”**

BYUNGKI RYU<sup>†,\*</sup>, JAYWAN CHUNG<sup>†,\*</sup>, AND SUDONG PARK

1. THERMOELECTRIC PROPERTY DATA USED IN THE MANUSCRIPT

In this work, we constructed a dataset of TEPs of 276 materials gathered from 264 literatures [1–264] to test our method. The TEPs were digitized using the Plot Digitizer [265]. The dataset consists of Seebeck coefficient  $\alpha$ , electrical resistivity  $\rho$ , and thermal conductivity  $\kappa$  at measured temperature  $T$ . For the numerical computation of efficiency, we use the available temperature ranges of the given material: the  $T_c$  is defined as the maximum of the lowest measured temperature and  $T_h$  is defined as the minimum of the highest measured temperature for given materials.

As shown in Table S1, the 276 materials in our dataset have various base-material groups: 59 Bi<sub>2</sub>Te<sub>3</sub>-related materials, 55 PbTe-related materials, 40 skutterudite (SKD), 23 Mg<sub>2</sub>Si-based materials, 18 GeTe materials, 14 M<sub>2</sub>Q antifluorite-type chalcogenide materials (where M = Cu, Ag, Au and Q = Te, Se), 12 SnTe-related materials, 11 ABQ<sub>2</sub>-type materials (where A=Group I, B=Bi, Sb, Q=Te, Se), 8 SnSe-related materials, 7 PbSe-related materials, 7 half-Heusler (HH) materials, 6 SiGe-related materials, 3 In<sub>4</sub>Se<sub>3</sub>-related materials, 3 PbS-related materials, 2 oxide materials, 2 clathrate materials, and 6 others. Here the base-material denotes the representative material, not the exact composition. Also note that for the categorization of base materials, the doping element is ignored. For examples, Bi<sub>2</sub>Te<sub>3</sub>, Sb<sub>2</sub>Te<sub>3</sub>, Bi<sub>2</sub>Se<sub>3</sub> binary and their ternary alloys are categorized as Bi<sub>2</sub>Te<sub>3</sub>-related materials. The material doping composition is not denoted in the composition of the base material.

For the segmented-leg devices, we consider 18 candidates showing high peak  $zT$  values exceeding 1. The full  $zT$  curves of them are shown in Figure S1. Table S2, S3 and S4 contain more information of the materials, including available temperature range, peak  $zT$ , numerical efficiency, formula efficiency, and the thermoelectric degrees of freedom.

---

(B Ryu, J Chung, and SD Park) ENERGY CONVERSION RESEARCH CENTER, KOREA ELECTROTECHNOLOGY RESEARCH INSTITUTE (KERI), 12, BULMOSANRO 10BEON-GIL, SEONGSAN-GU, CHANGWON, 51543, REPUBLIC OF KOREA

(<sup>†</sup>) B.R. AND J.C. CONTRIBUTED EQUALLY TO THIS WORK

*E-mail addresses:* byungkiryu@keri.re.kr, jchung@keri.re.kr, john@keri.re.kr.

*Date:* March 30, 2023.

TABLE S1. TEP Dataset of 276 materials with various material groups. ‘Group’ and ‘#mat.’ columns represent the group of base material and the number of materials inside the Group.

Group	#mat.	Group	#mat.
Bi <sub>2</sub> Te <sub>3</sub>	59	SnSe	8
PbTe	55	PbSe	7
SKD	40	HH	7
Mg <sub>2</sub> Si	23	SiGe	6
GeTe	18	In <sub>4</sub> Se <sub>3</sub>	3
M <sub>2</sub> Q	14	PbS	3
SnTe	12	Oxide	2
ABQ <sub>2</sub>	11	clathrate	2
etc.	6	<b>Total</b>	<b>276</b>

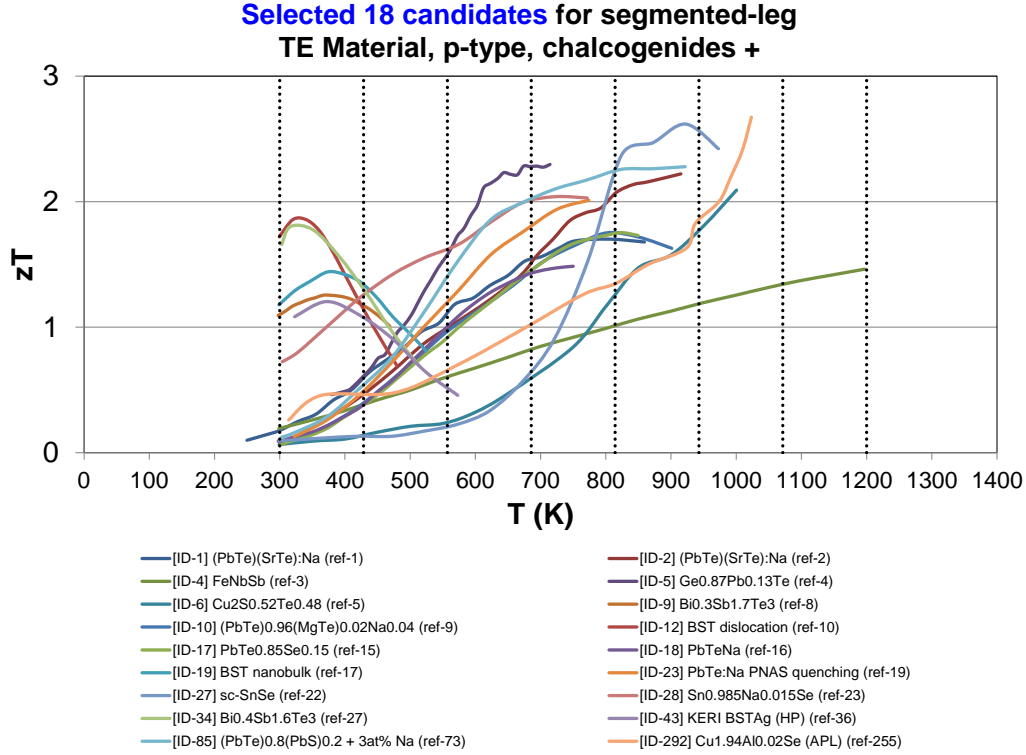


FIGURE S1. The  $zT$  curves for 18 selected materials. The ‘ref-#’ is the reference number.

TABLE S2. Information of 18 selected materials: available temperature range  $T_c$  and  $T_h$ ,  $\Delta T = T_h - T_c$ , peak  $zT$ , temperature of the peak  $zT$ .

ID-#	Material or Process [Reference]	$T_c$ (K)	$T_h$ (K)	peak- $zT$ @ $T$
ID-1	(PbTe)(SrTe):Na [1]	251	818	1.7 @800K
ID-2	(PbTe)(SrTe):Na [2]	302	915	2.2 @915K
ID-4	FeNbSb [3]	301	1200	1.5 @1200K
ID-5	Ge <sub>0.87</sub> Pb <sub>0.13</sub> Te [4]	329	713	2 @673K
ID-6	Cu <sub>2</sub> S <sub>0.52</sub> Te <sub>0.48</sub> [5]	299	997	2.1 @1000K
ID-9	Bi <sub>0.3</sub> Sb <sub>1.7</sub> Te <sub>3</sub> [8]	298	479	1.3 @380K
ID-10	(PbTe) <sub>0.96</sub> (MgTe) <sub>0.02</sub> Na <sub>0.04</sub> [9]	307	900	1.8 @810K
ID-12	BST dislocation [10]	300	480	1.86 @320K
ID-17	PbTe <sub>0.85</sub> Se <sub>0.15</sub> [15]	300	847	1.8 @850K
ID-18	PbTeNa [16]	300	750	1.4 @750K
ID-19	BST nanobulk [17]	300	525	1.4 @373K
ID-23	PbTe:Na, quenching (PNAS) [19]	321	759	2 @773K
ID-27	sc-SnSe, <i>b</i> -axis [22]	303	970	2.6 @923K
ID-28	Sn <sub>0.985</sub> Na <sub>0.015</sub> Se [23]	304	773	2 @773K
ID-34	Bi <sub>0.4</sub> Sb <sub>1.6</sub> Te <sub>3</sub> [27]	303	513	1.8 @316K
ID-43	KERI BSTAg, HP [36]	323	573	1.2 @373K
ID-85	(PbTe) <sub>0.8</sub> (PbS) <sub>0.2</sub> + 3at% Na [73]	302	922	2.3 @923K
ID-292	Cu <sub>1.94</sub> Al <sub>0.02</sub> Se (APL) [255]	327	1019	2.62 @1029K

TABLE S3. Information of 18 selected materials: (a) maximum efficiencies computed using exact numerical method ( $T$  is computed by fixed-point iteration, then power, heat and efficiency are computed), maximum efficiencies computed from general maximum efficiency formula  $\eta_{\max}^{\text{gen}}$  (see equation (15)) (b) using *exact* thermoelectric degrees of freedom (DOFs) with exact  $T$  ( $Z_{\text{gen}}, \tau, \beta$ ), (c) using DOFs with  $T^{(0)}$  ( $Z_{\text{gen}}^{(0)}, \tau^{(0)}, \beta^{(0)}$ ), (d) using DOFs with *one-shot* approximation ( $Z_{\text{gen}}^{(0)}, \tau_{\text{lin}}^{(0)}, \beta_{\text{lin}}^{(0)}$ ), (e) using DOFs with only  $Z_{\text{gen}}$  while  $\tau = \beta = 0$ , (f) using DOFs with only  $Z_{\text{gen}}^{(0)}$  while  $\tau = \beta = 0$ , and (g) using the classical efficiency formula for constant TEP using peak  $zT$ . Note that when we compute the numerical maximum efficiency we calculate the  $T$  using the fixed-point iteration with integral equation of  $T$  for given  $J$ . Then  $J$  is optimized to maximize the efficiency. Note that when we use the general maximum efficiency formula, the  $T$  and  $J$  are simultaneously computed. For  $T$ , the fixed-point iteration is used. For  $J$ , we use the optimal  $\gamma$  formula  $\gamma_{\max}^{\text{gen}}$ .

ID-#	$\eta_{\max}$						
	(a) exact	$\eta_{\max}^{\text{gen}}$					$\eta_{\max}^{\text{const}}$ (g) peak $zT$
		(b) $Z_{\text{gen}}, \tau, \beta$	(c) $Z_{\text{gen}}^{(0)}, \tau^{(0)}, \beta^{(0)}$	(d) $Z_{\text{gen}}^{(0)}, \tau_{\text{lin}}^{(0)}, \beta_{\text{lin}}^{(0)}$	(e) $Z_{\text{gen}}$	(f) $Z_{\text{gen}}^{(0)}$	
ID-1	13.7%	13.7%	14.4%	14.3%	14.5%	15%	22.9%
ID-2	15.9%	15.9%	16.2%	16.1%	16.6%	16.8%	24.9%
ID-4	15.3%	15.3%	15.8%	15.8%	15.8%	16.3%	23.8%
ID-5	12.5%	12.6%	12.9%	13%	13.1%	13.4%	18%
ID-6	10.5%	10.5%	10.7%	10.7%	11.1%	11.1%	25.9%
ID-9	8.4%	8.4%	8.4%	8.4%	8.4%	8.4%	9.2%
ID-10	13.8%	13.8%	14.2%	14.1%	14.4%	14.7%	22%
ID-12	9.1%	9.1%	9.1%	9.1%	9%	9%	11.2%
ID-17	12.6%	12.7%	13%	12.9%	13.3%	13.5%	21.5%
ID-18	10.4%	10.4%	10.8%	10.8%	10.9%	11.2%	16.9%
ID-19	9.9%	9.9%	10%	10%	9.9%	9.9%	11.1%
ID-23	11.6%	11.6%	12.1%	12.1%	12.2%	12.5%	19.6%
ID-27	7.1%	7.1%	7.1%	7.1%	7.1%	7.1%	27.9%
ID-28	16.2%	16.2%	16.9%	16.9%	16.7%	17.3%	20.9%
ID-34	10.1%	10.1%	10.1%	10.1%	10%	10%	12.2%
ID-43	8.2%	8.2%	8.2%	8.2%	8.1%	8.1%	10.3%
ID-85	17.6%	17.6%	18.1%	17.8%	18.5%	18.8%	25.6%
ID-292	14.3%	14.3%	14.9%	14.9%	14.9%	15.4%	27.5%

TABLE S4. Information of 18 selected materials: *exact* value and *one-shot* approximation of thermoelectric degrees of freedom.

ID-#	$Z_{\text{gen}}$	$\tau$	$\beta$	$Z_{\text{gen}}^{(0)}$	$\tau_{\text{lin}}^{(0)}$	$\beta_{\text{lin}}^{(0)}$
ID-1	0.0015	-0.253	0.192	0.0016	-0.207	0.199
ID-2	0.0018	-0.186	0.068	0.0018	-0.152	0.074
ID-4	0.0010	-0.164	0.197	0.0011	-0.141	0.203
ID-5	0.0022	-0.227	0.094	0.0023	-0.168	0.105
ID-6	0.0008	-0.253	0.027	0.0008	-0.208	0.028
ID-9	0.0029	-0.019	0.135	0.0029	-0.017	0.136
ID-10	0.0015	-0.192	0.102	0.0015	-0.161	0.107
ID-12	0.0033	0.030	0.177	0.0033	0.032	0.178
ID-17	0.0014	-0.231	0.109	0.0015	-0.189	0.112
ID-18	0.0014	-0.271	0.167	0.0014	-0.214	0.172
ID-19	0.0028	-0.015	0.189	0.0028	-0.013	0.190
ID-23	0.0017	-0.254	0.138	0.0017	-0.194	0.142
ID-27	0.0005	0.082	-0.379	0.0005	0.086	-0.382
ID-28	0.0025	-0.154	0.217	0.0026	-0.118	0.225
ID-34	0.0032	0.033	0.164	0.0032	0.036	0.166
ID-43	0.0019	0.028	0.186	0.0019	0.029	0.187
ID-85	0.0021	-0.179	0.079	0.0021	-0.146	0.095
ID-292	0.0013	-0.211	0.178	0.0014	-0.166	0.187

## 2. NUMERICAL EFFICIENCY CALCULATION IN FIGURE 1

Numerical maximum efficiencies of ideal thermoelectric devices without thermal loss by radiation or air convection are computed for 276 materials and compared with the peak  $zT$  values. The thermoelectric properties are *linearly interpolated* at intermediate temperatures. The exact temperature distribution  $T(x)$  of steady state is determined by solving the differential equations of thermoelectricity with Dirichlet boundary conditions; the end point temperature is determined from the available temperature range. Then the thermoelectric performances of a thermoelectric leg with length  $L$  and cross sectional area  $A$  are calculated as a function of current density  $J$  given as  $\eta(J) = \frac{P/A}{Q_h/A} = \frac{J(\int_c^h \alpha dT - J \int_0^L \rho dx)}{-\kappa_h \nabla T_h + J \alpha_h T_h}$ , where the  $P$  and  $Q_h$  are the power delivered outside and the hot-side heat current respectively. Then, the maximum of numerical efficiency ( $\eta_{\max}$ ) is calculated, which satisfies the relation  $\eta(J) \leq \eta_{\max}$ . The reduced efficiency  $\eta_{\text{red}}$  is obtained as  $\eta_{\text{red}} = \frac{\eta_{\max}}{\eta_{\text{Carnot}}}$ , where  $\eta_{\text{Carnot}} = \frac{T_h - T_c}{T_h}$ .

## 3. DEVICE PARAMETERS AND OPERATING CONDITIONS

The thermoelectric (TE) power device mentioned in this paper is a uni-leg device composed of a single leg or a segmented leg sandwiched by heat source ( $T_h$ ) and heat sink ( $T_c$ ) at both sides. In such a device, electric current and heat current flow simultaneously across the leg. For the simplicity, we assume the steady-state condition. For  $p$ -type material ( $\alpha > 0$ ), the electric current and the heat current flow in the same direction from hot to cold side, while the direction of the electric current is reversed in  $n$ -type material ( $\alpha < 0$ ).

The most important parameters in a TE device are voltage  $V$ , electrical resistance  $R$ , and thermal resistance  $1/K$ , which can describe the electrical and thermal circuits of the TE device. Once these three device parameters are known, we can roughly estimate the thermoelectric performance of the TE device. When there is load resistance  $R_L$ , there will be electric current  $I = \frac{V}{R+R_L}$ . When there is no electric current, there will be heat current  $Q_h = -A\kappa\nabla T = K\Delta T$ . When there is non-zero electric current, there will be heat generation by Thomson and Joule heat and the hot side heat current will be approximately  $Q_h \approx K\Delta T + I\frac{V}{\Delta T}T_h - \frac{1}{2}I^2R$ . The approximation becomes exact when there is no temperature dependency in thermoelectric properties (TEPs). The three parameters  $V, R, K$  are easily determined from the TE properties. Note that a leg of the device is equivalent to a series of infinitesimal parts  $dx$ , and it is trivial to write the induced open-circuit voltage ( $V$ ) as an integration of  $-\alpha\nabla T$  on  $x$ , and the resistance of the TE leg ( $R_{TE}$  and  $1/K_{TE}$ ) as an integration of resistivity  $\rho$  and  $1/\kappa$  on  $x$ ; see Figure S2. Also note that the electrical and thermal resistances should be calculated by integration of the corresponding resistivities on  $x$ , not on  $T$ .

When the material thermoelectric figure of merit  $zT$  is small, the electric current density  $J$  is so small that the  $R$  and  $K$  can be estimated by  $R^{(0)}$  and  $K^{(0)}$  which are the electrical resistance and thermal conductance for zero-current-density case ( $J = 0$ ). Similarly, since the  $J$  is small, the temperature can be estimated by the zero-current-density solution  $T^{(0)}(x)$  which is the solution of the heat equation  $\nabla \cdot (\kappa\nabla T) = 0$  without thermoelectric heat generation. Here the  $\kappa$  is thermal conductivity. The heat flows are nearly the same along the thermoelectric leg so the one-dimensional heat equation suggests  $\kappa \frac{dT}{dx}$

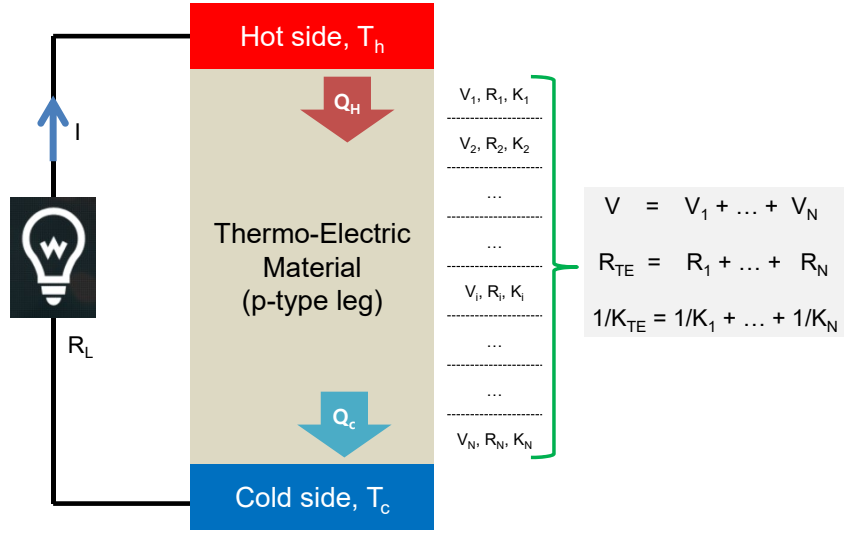


FIGURE S2. Structure of conventional thermoelectric power devices. For simplicity, we draw only an uni-leg with  $p$ -type materials where electric current flows from hot to cold side. Since the electric current and heat current flow through the leg, the electrical and thermal resistance of the leg should be considered as the sum of an infinitesimal serial circuit. Thus, the voltage  $V$  and the resistance  $R$  should be the sum of component voltages and resistances respectively. In the case of thermal conduction, the inverse of thermal conductivity should be used for thermal circuit parameter.

is constant. Hence the average thermal conductivity  $\bar{\kappa}^{(0)}$  for  $J = 0$  satisfies  $\bar{\kappa}^{(0)} \frac{\Delta T}{L} = \kappa \frac{dT}{dx}$  so it can be evaluated by integration over  $T$ :  $\bar{\kappa}^{(0)} = \int \bar{\kappa}^{(0)} \frac{1}{L} dx = \frac{1}{\Delta T} \int \kappa \frac{dT}{dx} dx = \langle \kappa \rangle_T$  by the change of variable  $dx = \frac{\kappa dT}{\bar{\kappa}_0 \frac{\Delta T}{L}}$ . Here the  $\langle \kappa \rangle_T$  denotes the average of the thermal conductivity  $\kappa(T)$  over  $T$ . Meanwhile, the resistivity under the condition of  $J = 0$  is calculated as  $\bar{\rho}^{(0)} = \frac{1}{L} \int \rho dx = \frac{1}{L} \int \rho \frac{\kappa dT}{\bar{\kappa}^{(0)} \frac{\Delta T}{L}} = \frac{1}{\bar{\kappa}^{(0)} \Delta T} \int \rho \kappa dT = \frac{\langle \rho \kappa \rangle_T}{\langle \kappa \rangle_T}$ . Finally we may rewrite  $RK = \bar{\rho} \bar{\kappa} \approx \bar{\rho}^{(0)} \bar{\kappa}^{(0)} = \langle \rho \kappa \rangle_T$  under small  $zT$ .

The above idea to use the device parameters for  $J = 0$  is the main idea of the one-shot approximation, of which argument is dealt thoroughly in §10. Every thermoelectric material at the moment has the peak  $zT$  smaller than 3, implying that the above idea gives a good approximation  $Z_{\text{gen}}^{(0)}$  for  $Z_{\text{gen}}$ ; see (17) for its definition. However, under large  $zT$  or non-zero  $J$ , the approximation  $Z_{\text{gen}}^{(0)}$  may have 1 to 10 percent error.

#### 4. THERMOELECTRIC DIFFERENTIAL EQUATION IN ONE-DIMENSION

The thermoelectric effect is expressed in terms of electric current density  $J$  and heat current density  $J^Q$ :  $J = \sigma(E - \alpha \nabla T)$  and  $J^Q = \alpha T J - \kappa \nabla T$  where  $E$  is electric field. Applying the energy conservation law on  $J$  and  $J^Q$  and assuming *one-dimensional* circuit case, we can obtain the thermoelectric differential equation [266, 267] describing evolution



of temperature distribution  $T(x)$  inside an uni-leg thermoelectric device:

$$(1) \quad \frac{d}{dx} \left( \kappa \frac{dT}{dx} \right) + \rho J^2 - T \frac{d\alpha}{dT} \frac{dT}{dx} J = 0$$

where  $x$  is coordinate inside the one-dimensional thermoelectric leg. We have Dirichlet boundary condition since the temperatures at the end of the leg are fixed:

$$(2) \quad T(0) = T_h, \quad T(L) = T_c.$$

In the one-dimensional leg, where the cross sectional area  $A$  is constant across the leg, the electric current is calculated as  $I = J \times A$  and the heat current is calculated as  $Q = J^Q \times A$

### 5. AVERAGE PARAMETERS AND GENERAL FIGURE OF MERIT $Z_{\text{gen}}$

To analyze the thermoelectric equation (1), the following average material properties are helpful:

$$\begin{aligned} \bar{\alpha} &:= \frac{1}{\Delta T} \int_{T_c}^{T_h} \alpha dT = \frac{V}{\Delta T}, \\ \bar{\rho} &:= \frac{1}{L} \int_0^L \rho dx = \frac{A}{L} R, \\ \frac{1}{\bar{\kappa}} &:= \frac{1}{L} \int_0^L \frac{1}{\kappa} dx = \frac{A}{L} \frac{1}{K}. \end{aligned}$$

Note the average parameters give the induced open-circuit voltage  $V$ , electrical resistance  $R$  and thermal resistance  $1/K$  of the leg. Using these parameters we also define the *general device figure of merit*  $Z_{\text{gen}}$  for temperature dependent material properties:

$$(3) \quad Z_{\text{gen}} := \frac{\bar{\alpha}^2}{RK} = \frac{\bar{\alpha}^2}{\bar{\rho}\bar{\kappa}},$$

which generalize the classical device figure of merit. If the material properties are temperature independent, the  $Z_{\text{gen}}$  is reduced to the conventional material parameter  $z$ .

### 6. ELECTRIC CURRENT EQUATION

With given load resistance  $R_L$ , an equation for the electric current density  $J = \sigma \left( E - \alpha \frac{dT}{dx} \right)$  can be found by integrating  $\rho J$  along the closed circuit:  $\oint \rho J dx = \oint E dx - \oint \alpha \frac{dT}{dx} dx = V$ . Hence the electric current  $I$  satisfies  $(R + R_L)I = V$  and we have

$$(4) \quad J = \frac{1}{A} \frac{V}{R + R_L}.$$

Note that the  $R = \frac{1}{A} \int_0^L \rho(T(x)) dx$  depends on  $T$  so does the  $J$ .

### 7. INTEGRAL EQUATIONS OF $T(x)$ AND $\nabla T(x)$

Due to the nonlinearity ( $\kappa, \alpha, \rho$  depend on  $T$ ) and nonlocality ( $J$  depends on an integral of  $T$ ) [266], the equation (1) does not have an analytic solution. Instead, we rewrite the equation as an integral form where fixed-point iteration is possible. The integral equation will give us physical insights to derive the remaining degrees of freedom  $\tau$  and  $\beta$ .

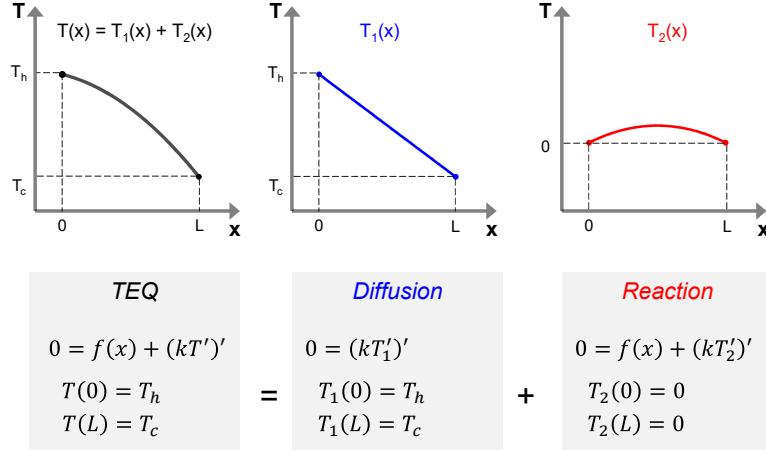


FIGURE S3. Crucial idea to solve the temperature equation. The solution of the PDE (1) can be decomposed to  $T_1(x)$  and  $T_2(x)$  with proper boundary conditions. Without the reaction term, the solution becomes simple, while still having physical meaning due to the relatively small contribution of  $T_2(x)$  in thermoelectric legs.

For simplicity, we denote the term with Joule heat and Thomson heat by  $f_T(x)$ :

$$(5) \quad f_T(x) := \rho J^2 - T \frac{d\alpha}{dT} \frac{dT}{dx} J.$$

Then the equation (1) is  $\frac{d}{dx} \left( \kappa \frac{dT}{dx} \right) + f_T = 0$ . If the solution  $T_{\text{sol}}$  of (1), (2), (4) is known, we may put  $\kappa(x) := \kappa(T_{\text{sol}}(x))$  and  $f(x) := f_{T_{\text{sol}}}(x)$  to find a *linear* equation

$$(6) \quad \frac{d}{dx} \left( \kappa(x) \frac{dT}{dx} \right) + f = 0.$$

Since this equation is linear, we can find a solution by decomposing it into a homogeneous solution  $T_1$  and particular solution  $T_2$ :  $T = T_1 + T_2$ . The  $T_1$  and  $T_2$  are solutions of

$$(7) \quad \frac{d}{dx} \left( \kappa(x) \frac{dT_1}{dx} \right) = 0, \quad T_1(0) = T_h, \quad T_1(L) = T_c,$$

$$(8) \quad \frac{d}{dx} \left( \kappa(x) \frac{dT_2}{dx} \right) + f = 0, \quad T_2(0) = 0, \quad T_2(L) = 0.$$

This idea is summarized in Figure S3. To solve the equation (7), we integrate it over  $x$  to yield  $\kappa(x) \frac{dT_1}{dx}(x) = C$  for some constant  $C$ . Dividing both sides by  $\kappa$  and integrating from 0 to  $x$ , we have  $T_1(x) - T_1(0) = C \int_0^x \frac{1}{\kappa(x)} dx$ . Imposing the boundary conditions yields  $C = -K \frac{T_h - T_c}{A}$  and

$$T_1(x) = T_h - \frac{K \Delta T}{A} \int_0^x \frac{1}{\kappa(x)} dx.$$

To solve the equation (8), we integrate it from 0 to  $x$  to yield  $\kappa(x)\frac{dT_2}{dx}(x) - C = -\int_0^x f(s) ds =: -F(x)$  for some constant  $C$ . Dividing both sides by  $\kappa$  and integrating from 0 to  $x$ , we have  $T_2(x) - T_2(0) = -\int_0^x \frac{F(x)}{\kappa(x)} dx + C \int_0^x \frac{1}{\kappa(x)} dx$ . Imposing the zero boundary conditions yields

$$T_2(x) = -\int_0^x \frac{F(x)}{\kappa(x)} dx + \frac{K \delta T}{A} \int_0^x \frac{1}{\kappa(x)} dx,$$

where  $\delta T := \int_0^L \frac{F(x)}{\kappa(x)} dx$  is a scalar quantity.

Summing up, we have the solution  $T = T_1 + T_2$  of (6), (2) and its gradient:

$$(9) \quad T(x) = \left( T_h - \frac{K \Delta T}{A} \int_0^x \frac{1}{\kappa} dx \right) + \left( -\int_0^x \frac{F(x)}{\kappa(x)} dx + \frac{K \delta T}{A} \int_0^x \frac{1}{\kappa} dx \right)$$

$$(10) \quad \frac{dT}{dx}(x) = \left( -\frac{K \Delta T}{A} \frac{1}{\kappa(x)} \right) + \left( \frac{F(x)}{\kappa(x)} + \frac{K \delta T}{A} \frac{1}{\kappa(x)} \right)$$

where  $F(x) = \int_0^x f(s) ds$  and  $\delta T = \int_0^L \frac{F(x)}{\kappa(x)} dx$ . Since  $\kappa(x) = \kappa(T(x))$  and  $f(x) = f_T(x)$ , the equation (9) is an integral form  $T = \varphi[T]$  where  $\varphi$  is the integral operator in the right-hand side of (9).

To find  $T$ , we apply fixed-point iteration [268] to the relation  $T = \varphi[T]$ . Choosing an initial guess  $T_0$  for  $T$  (it can be a linear distribution satisfying Dirichlet condition or the temperature curve satisfying  $J = 0$ ), we iteratively compute a sequence of functions  $T_{n+1} = \varphi[T_n]$  for  $n \geq 0$ . Then we expect  $T_n$  converges to a function  $T_\infty$  which is the solution we are looking for because it satisfies  $T_\infty = \varphi[T_\infty]$ . Computation reveals that with linear  $T_0$ , the  $T_n$  converges enough within a few iterations (less than 10 iterations).

## 8. HEAT CURRENT AND ADDITIONAL FIGURE OF MERIT $\tau$ AND $\beta$

Using the  $\frac{dT}{dx}$  in (10), the hot-side heat current can be written as

$$(11) \quad Q_h = A J_h^Q = I \alpha_h T_h - A \kappa_h \left( \frac{dT}{dx} \right)_h = I \alpha_h T_h + K(\Delta T - \delta T).$$

Now we decompose  $\delta T$  into two terms having  $I$  and  $I^2$ . From (5),

$$\begin{aligned} F_T(x) &= \int_0^x f_T(s) ds = I^2 \int_0^x \frac{1}{A^2} \rho(s) ds - I \int_0^x \frac{1}{A} T(s) \frac{d\alpha}{dT}(T(s)) \frac{dT}{dx}(s) ds \\ &=: I^2 F_T^{(2)}(x) - I F_T^{(1)}(x). \end{aligned}$$

Hence

$$\begin{aligned} \delta T &= \int_0^L \frac{F_T(x)}{\kappa(x)} dx = I^2 \int_0^L \frac{F_T^{(2)}(x)}{\kappa(x)} dx - I \int_0^L \frac{F_T^{(1)}(x)}{\kappa(x)} dx \\ &=: I^2 \delta T^{(2)} - I \delta T^{(1)}. \end{aligned}$$

For *temperature-independent* material properties, we can easily check that  $\delta T^{(2)} = \frac{1}{2} \frac{R}{K}$  and  $\delta T^{(1)} \equiv 0$  so that the hot-side heat current is

$$\overline{Q}_h = K \Delta T + I \bar{\alpha} T_h - \frac{1}{2} I^2 R.$$

Our strategy is to consider the  $Q_h$  in (11) as a perturbation of  $\overline{Q}_h$  above. To do so, we replace  $\alpha_h$  by  $\bar{\alpha}$  in (11) and introduce dimensionless perturbation parameters  $\tau$  and  $\beta$  of

which values become zero for temperature-independent material properties. Precisely we let

$$(12) \quad \begin{aligned} \tau &:= \frac{1}{\bar{\alpha}\Delta T} [(\bar{\alpha} - \alpha_h)T_h - K \delta T^{(1)}], \\ \beta &:= \frac{2}{R} K \delta T^{(2)} - 1. \end{aligned}$$

Then we can rewrite the  $Q_h$  in (11) by

$$(13) \quad Q_h = K\Delta T + I\bar{\alpha}(T_h - \tau\Delta T) - \frac{1}{2}I^2R(1 + \beta).$$

Observing the delivered power  $P = I(V - IR) = I(\bar{\alpha}\Delta T - IR)$  is equal to  $Q_h - Q_c$ , we have the cold-side heat current:

$$Q_c = K\Delta T + I\bar{\alpha}(T_c - \tau\Delta T) + \frac{1}{2}I^2R(1 - \beta).$$

When the average device parameters are fixed, the  $Q_h$  in (13) decreases as  $\tau$  or  $\beta$  increases while the delivered power  $P$  is fixed. Hence the efficiency  $\eta = \frac{P}{Q_h}$  increases as  $\tau$  or  $\beta$  increases. This implies each of  $\tau$  and  $\beta$  is a figure of merit for efficiency, as well as  $Z_{\text{gen}}$  is.

## 9. EFFICIENCY PREDICTION USING THERMOELECTRIC DEGREES OF FREEDOM

Here we derive an efficiency formula in terms of the thermoelectric degrees of freedom  $Z_{\text{gen}}$ ,  $\tau$ ,  $\beta$  and find the maximum efficiency. Let  $\gamma := \frac{R_L}{R}$ . Then the electric current is  $I = \frac{\bar{\alpha}\Delta T}{R(1+\gamma)}$  and the delivered power is  $P = I(\bar{\alpha}\Delta T - IR) = \frac{(\bar{\alpha}\Delta T)^2}{R} \frac{\gamma}{(1+\gamma)^2}$ . Using (13), the efficiency  $\eta = \frac{P}{Q_h} = \frac{P/(K\Delta T)}{Q_h/(K\Delta T)}$  can be written as

$$\eta(Z_{\text{gen}}, \tau, \beta | T_h, T_c, \gamma) = \frac{Z_{\text{gen}}\Delta T \frac{\gamma}{(1+\gamma)^2}}{1 + Z_{\text{gen}}\left(\frac{1}{1+\gamma}\right)(T_h - \tau\Delta T) - \frac{1}{2}Z_{\text{gen}}\Delta T\left(\frac{1}{1+\gamma}\right)^2(1 + \beta)}.$$

We can easily check that the efficiency is monotonic on  $Z_{\text{gen}}$ ,  $\tau$  and  $\beta$  for fixed  $T_h, T_c$  and  $\gamma$ . Assuming  $Z_{\text{gen}}, \tau, \beta$  changes little near the  $\gamma$  at the maximum efficiency, we solve  $\frac{\partial \eta}{\partial \gamma} = 0$  to estimate the maximum efficiency. For simplicity, we let

$$T'_h := T_h - \tau\Delta T, \quad T'_c := T_c - (\tau + \beta)\Delta T, \quad T'_m := \frac{1}{2}(T'_h + T'_c).$$

Then the solution of  $\frac{\partial \eta}{\partial \gamma} = 0$  is

$$(14) \quad \gamma_{\text{max}}^{\text{gen}} = \sqrt{1 + Z_{\text{gen}}T'_m}.$$

Hence the maximum efficiency is approximated by

$$(15) \quad \eta_{\text{max}} \approx \eta_{\text{max}}^{\text{gen}} := \frac{\Delta T}{T'_h} \frac{\sqrt{1 + Z_{\text{gen}}T'_m} - 1}{\sqrt{1 + Z_{\text{gen}}T'_m} + \frac{T'_c}{T'_h}}.$$

This formula generalizes the classical maximum efficiency formula for temperature-independent material properties because it has the same form as the classical formula but predicts the exact maximum efficiency accurately; see Figure S6.

10. ONE-SHOT APPROXIMATION  $Z_{\text{gen}}^{(0)}$ ,  $\tau_{\text{lin}}^{(0)}$  AND  $\beta_{\text{lin}}^{(0)}$ 

The computation of  $Z_{\text{gen}}$ ,  $\tau$  and  $\beta$  requires the exact temperature distribution. But they can be estimated directly from the material properties. In this section we derive an approximate formula for  $Z_{\text{gen}}$ ,  $\tau$  and  $\beta$ . The idea is to use the temperature distribution for  $J = 0$ , which is similar to the exact temperature distribution because most devices induce small  $J$  due to the small  $zT$ . Let  $T^{(0)}$  be the temperature distribution for  $J = 0$  and define

$$\begin{aligned}\bar{\rho}^{(0)} &:= \frac{1}{L} \int_0^L \rho(T^{(0)}(x)) dx = \frac{A}{L} R^{(0)}, \\ \frac{1}{\bar{\kappa}^{(0)}} &:= \frac{1}{L} \int_0^L \frac{1}{\kappa(T^{(0)}(x))} dx = \frac{A}{L} \frac{1}{K^{(0)}}.\end{aligned}$$

From (1) with  $J = 0$ , we can check that

$$(16) \quad -\kappa(T^{(0)}(x)) \frac{dT^{(0)}}{dx}(x) = \bar{\kappa}^{(0)} \frac{\Delta T}{L}.$$

Hence

$$\begin{aligned}\int_{T_c}^{T_h} \rho(T) \kappa(T) dT &= \int_{T_c}^{T_h} \rho(T^{(0)}) \left( -\frac{\Delta T}{L} \bar{\kappa}^{(0)} \right) \frac{dx}{dT^{(0)}} dT^{(0)} \\ &= \frac{\Delta T}{L} \int_0^L \rho(T^{(0)}(x)) \bar{\kappa}^{(0)} dx \\ &= \Delta T \bar{\rho}^{(0)} \bar{\kappa}^{(0)}.\end{aligned}$$

Replacing  $T$  with  $T^{(0)}$  in  $Z_{\text{gen}} = \frac{\bar{\alpha}^2}{\bar{\rho}\bar{\kappa}}$ , we have an one-shot approximation for  $Z_{\text{gen}}$ :

$$(17) \quad Z_{\text{gen}} \approx \frac{\bar{\alpha}^2}{\bar{\rho}^{(0)} \bar{\kappa}^{(0)}} = \frac{(\int \alpha dT)^2}{\Delta T \int \rho \kappa dT} =: Z_{\text{gen}}^{(0)}.$$

To approximate  $\tau$ , we assume the Seebeck coefficient is a linear function of  $T$ :

$$\alpha(T) \approx \alpha_{\text{lin}}(T) := \alpha_h + \left( \frac{\alpha_c - \alpha_h}{T_c - T_h} \right) (T - T_h).$$

In this way we can observe the effect of the gradient of  $\alpha$  on  $\tau$  more clearly. Since the  $\tau$  in (12) has  $K \delta T^{(1)}$  term, we estimate a relevant term:

$$\begin{aligned}F_T^{(1)}(s) &\approx \int_0^s \frac{1}{A} T \frac{d\alpha_{\text{lin}}}{dT}(T(x)) \frac{dT}{dx} dx = \int_{T_h}^{T(s)} \frac{1}{A} T \frac{\alpha_c - \alpha_h}{T_c - T_h} dT \\ &= \frac{1}{2A} \frac{\alpha_c - \alpha_h}{T_c - T_h} (T(s)^2 - T_h^2) =: \widehat{F}^{(1)}(T(s)).\end{aligned}$$

Using  $-\kappa \frac{dT}{dx} \approx \bar{\kappa}^{(0)} \frac{\Delta T}{L}$  from (16),

$$\begin{aligned} \delta T^{(1)} &= \int_0^L \frac{F_T^{(1)}(x)}{\kappa(x)} dx \approx - \int_0^L \frac{\widehat{F}^{(1)}(T(x))}{\bar{\kappa}^{(0)}} \frac{L}{\Delta T} \frac{dT}{dx} dx \\ &= \frac{1}{\bar{\kappa}^{(0)}} \frac{L}{\Delta T} \int_{T_c}^{T_h} \widehat{F}^{(1)}(T) dT \\ &= \frac{1}{2K^{(0)}} \frac{1}{\Delta T} \frac{\alpha_c - \alpha_h}{T_c - T_h} \frac{1}{3} (\Delta T)^2 (-3T_h + \Delta T) \\ &= \frac{\alpha_h - \alpha_c}{6K^{(0)}} (-3T_h + \Delta T) =: \widehat{\delta T}^{(1)} \end{aligned}$$

where  $K^{(0)} := \frac{A}{L} \bar{\kappa}^{(0)}$ . Therefore we have an one-shot approximation for  $\tau$ :

$$\begin{aligned} \tau &\approx \frac{1}{\alpha_{\text{lin}} \Delta T} \left[ (\bar{\alpha}_{\text{lin}} - \alpha_h) T_h - K^{(0)} \widehat{\delta T}^{(1)} \right] \\ &= -\frac{1}{3} \frac{\alpha_h - \alpha_c}{\alpha_h + \alpha_c} =: \tau_{\text{lin}}^{(0)}. \end{aligned}$$

To approximate  $\beta$ , we assume the  $\rho\kappa$  is a linear function of  $T$ :

$$(\rho\kappa)(T) \approx (\rho\kappa)_{\text{lin}}(T) := (\rho\kappa)_h + \left( \frac{(\rho\kappa)_c - (\rho\kappa)_h}{T_c - T_h} \right) (T - T_h).$$

Using  $-\kappa \frac{dT}{dx} \approx \bar{\kappa}^{(0)} \frac{\Delta T}{L}$  from (16), we approximate relevant terms for  $\beta$ :

$$\begin{aligned} F_T^{(2)}(s) &= \int_0^s \frac{1}{A^2} (\rho\kappa)(T(x)) \frac{1}{\kappa(x)} dx \approx \frac{-L}{A^2 \bar{\kappa}^{(0)} \Delta T} \int_0^s (\rho\kappa)_{\text{lin}}(T(x)) \frac{dT}{dx} dx \\ &= \frac{-L}{A^2 \bar{\kappa}^{(0)} \Delta T} \int_{T_h}^{T(s)} (\rho\kappa)_{\text{lin}}(T) dT \\ &= \frac{-L}{A^2 \bar{\kappa}^{(0)} \Delta T} \left[ (\rho\kappa)_h (T(s) - T_h) + \frac{1}{2} \frac{(\rho\kappa)_c - (\rho\kappa)_h}{T_c - T_h} (T(s) - T_h)^2 \right] \\ &=: \widehat{F}^{(2)}(T(s)) \end{aligned}$$

hence

$$\begin{aligned} \delta T^{(2)} &= \int_0^L \frac{F_T^{(2)}(x)}{\kappa(x)} dx \approx \int_0^L \widehat{F}^{(2)}(T(x)) \left( -\frac{L}{\bar{\kappa}^{(0)} \Delta T} \right) \frac{dT}{dx} dx \\ &= \frac{-L}{\bar{\kappa}^{(0)} \Delta T} \int_{T_h}^{T_c} \widehat{F}^{(2)}(T) dT \\ &= \frac{1}{6(K^{(0)})^2} (2(\rho\kappa)_h + (\rho\kappa)_c) =: \widehat{\delta T}^{(2)}. \end{aligned}$$

Therefore we have an one-shot approximation for  $\beta$ :

$$\begin{aligned} \beta &\approx \frac{2}{\frac{L}{A} \bar{\rho}^{(0)}} K^{(0)} \widehat{\delta T}^{(2)} - 1 = \frac{1}{3 \bar{\rho}^{(0)} \bar{\kappa}^{(0)}} (2(\rho\kappa)_h + (\rho\kappa)_c) - 1 \\ &\approx \frac{1}{\frac{3}{2} ((\rho\kappa)_h + (\rho\kappa)_c)} (2(\rho\kappa)_h + (\rho\kappa)_c) - 1 \\ &= \frac{1}{3} \frac{(\rho\kappa)_h - (\rho\kappa)_c}{(\rho\kappa)_h + (\rho\kappa)_c} =: \beta_{\text{lin}}^{(0)}. \end{aligned}$$

In summary, we have one-shot approximations as following:

$$(18) \quad Z_{\text{gen}} \approx Z_{\text{gen}}^{(0)} \equiv \frac{(\int \alpha dT)^2}{\Delta T \int \rho \kappa dT}, \quad \tau \approx \tau_{\text{lin}}^{(0)} \equiv -\frac{1}{3} \frac{\alpha_h - \alpha_c}{\alpha_h + \alpha_c}, \quad \beta \approx \beta_{\text{lin}}^{(0)} \equiv \frac{1}{3} \frac{\rho_h \kappa_h - \rho_c \kappa_c}{\rho_h \kappa_h + \rho_c \kappa_c}.$$

The *one-shot approximation* derived above is accurate enough for many cases. See Figure S4, where we compare the exact  $Z_{\text{gen}}$ ,  $\tau$ ,  $\beta$  with their one-shot approximations for 276 materials.

Furthermore, these one-shot approximations can be used to predict the performance of *segmented* devices. In Figure S5, we consider a two-stage segmented leg with no contact resistance. The segmented leg consists of SnSe [22] for hot side and BiSbTe [17] for cold side. The exact temperature distribution  $T$  inside the leg shows a jump of the gradient at  $x = 0.6$  due to the inhomogeneity of the material; see Figure S5(b). Despite the nonlinearity of the  $T$ , the one-shot approximation using  $Z_{\text{gen}}^{(0)}$ ,  $\tau_{\text{lin}}^{(0)}$  and  $\beta_{\text{lin}}^{(0)}$ , which does not use the exact  $T$ , shows high accuracy in prediction of thermoelectric performances; see Figure S5(c)-(f). The relative error is high near  $\gamma = 0$ , where the reaction term is large due to the large electric current. For large  $\gamma$ , the error is negligible. Near the  $\gamma = 1$ , the error is acceptable; the relative error is less than 5%. The one-shot approximation predicts the maximum efficiency to be 7.68% while the exact value is 7.53%.

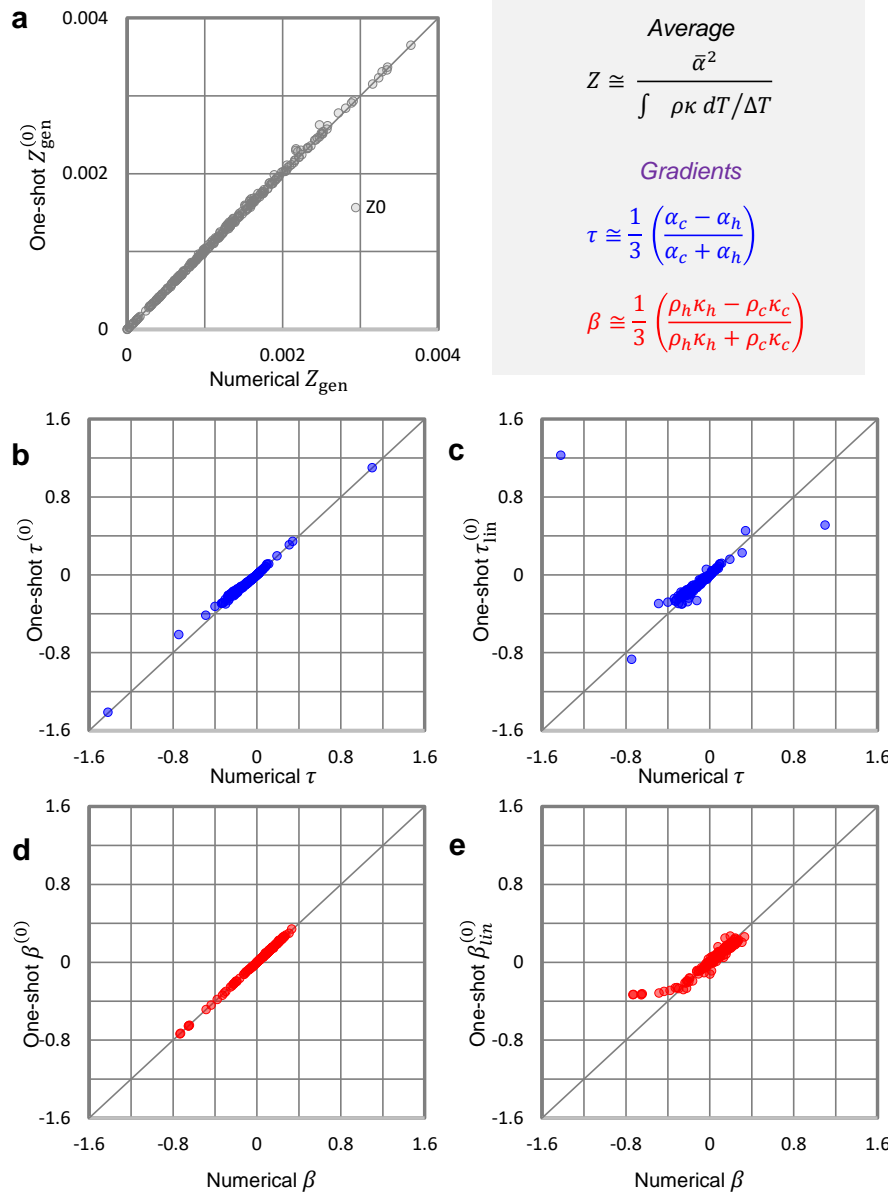


FIGURE S4. Estimation of thermoelectric degrees of freedom for 276 materials. Numerical  $Z_{\text{gen}}, \tau, \beta$  are computed using the exact  $T$  at the maximum efficiency. One-shot approximations  $Z_{\text{gen}}^{(0)}, \tau^{(0)}, \beta^{(0)}$  are computed using the  $T^{(0)}$  for  $J = 0$ . Going further, the  $\tau_{\text{lin}}^{(0)}$  and  $\beta_{\text{lin}}^{(0)}$  are computed by assuming the linearity of  $\alpha$  and  $\rho\kappa$ ; see (18) for their explicit formula.



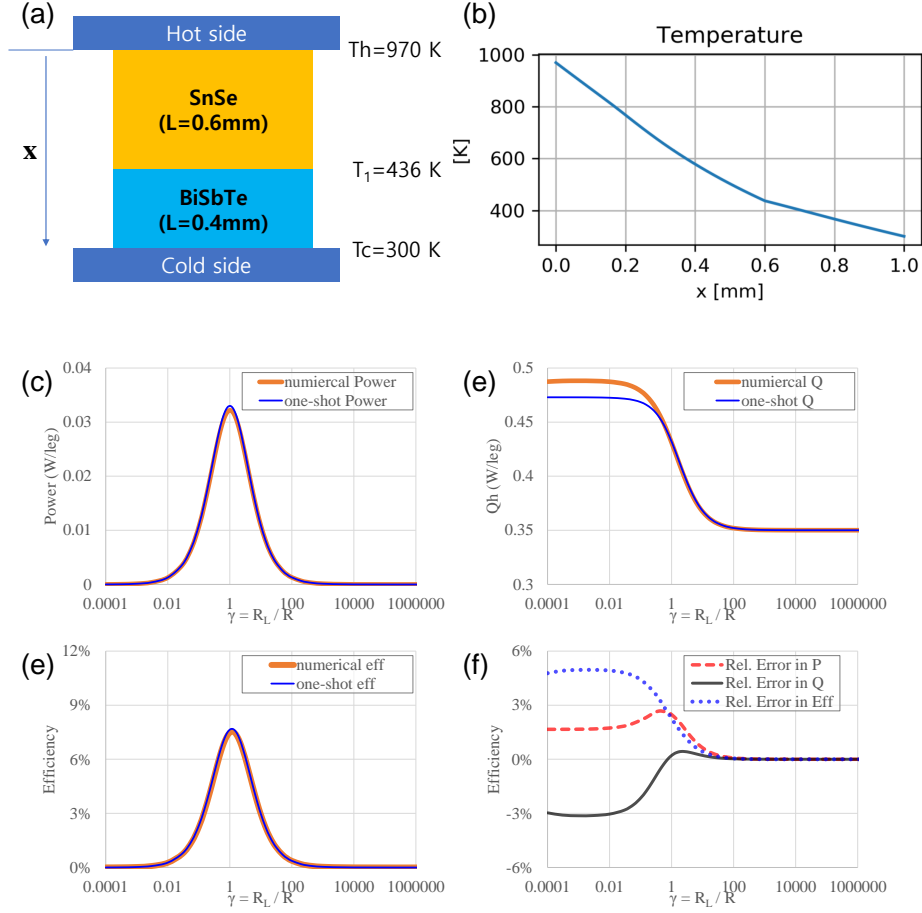


FIGURE S5. The thermoelectric performances of a two-stage segmented leg predicted by the one-shot approximation. The numerical exact values are computed by fixed-point iteration and the one-shot values are computed using  $Z_{\text{gen}}^{(0)}$ ,  $\tau_{\text{lin}}^{(0)}$  and  $\beta_{\text{lin}}^{(0)}$ ; see (18) for the explicit one-shot formula. (a) The geometry of the segmented leg: SnSe [22] and BiSbTe [17] are used for hot and cold-side materials.  $T_h = 970$  K and  $T_c = 300$  K are used. (b) Exact temperature distribution obtained by solving the integral equation (9) of  $T$  with fixed-point iteration. (c) Power delivered outside, (d) heat current at the hot side, (e) efficiency, and (f) relative errors in power, heat current, efficiency between the numerical value and the one-shot approximation.

11. MAXIMUM EFFICIENCY PREDICTION USING  $\eta_{\max}^{\text{gen}}$ 

In Figure S6, we can observe that the maximum efficiency estimation formula  $\eta_{\max}^{\text{gen}}(Z_{\text{gen}}, \tau, \beta)$  in (15) is highly accurate. In Table S5, various statistics on the relative error of maximum



FIGURE S6. Efficiency estimation for 276 materials using the formula  $\eta_{\max}^{\text{gen}}(Z_{\text{gen}}, \tau, \beta)$  in (15) and the peak  $zT$ . In use of  $\eta_{\max}^{\text{gen}}(Z_{\text{gen}}, \tau, \beta)$ , there are five options: using (i) exact  $Z_{\text{gen}}, \tau, \beta$  (Ztb), (ii)  $Z_{\text{gen}}^{(0)}, \tau^{(0)}, \beta^{(0)}$  (Z0t0b0), (iii)  $Z_{\text{gen}}^{(0)}, \tau_{\text{lin}}^{(0)}, \beta_{\text{lin}}^{(0)}$  (Z0t0linb0lin), (iv) exact  $Z_{\text{gen}}$  only,  $\tau = 0, \beta = 0$  (Z), (v)  $Z_{\text{gen}}^{(0)}$  only,  $\tau = 0, \beta = 0$  (Z0). (a) Comparison of the exact maximum efficiency and the estimations. (b) Relative error of the estimations (absolute error divided by the exact maximum efficiency). The peak  $zT$  is malfunctioning in efficiency prediction; the relative error can be over 100%. On the other hand, the formula  $\eta_{\max}^{\text{gen}}(Z_{\text{gen}}, \tau, \beta)$  has small relative error; even the simplest formula with  $Z_{\text{gen}}^{(0)}, \tau_{\text{lin}}^{(0)}, \beta_{\text{lin}}^{(0)}$  has the standard error (=root mean square of relative errors) less than 2%. See Table S5 for detailed values.

efficiency ( $\frac{\eta_{\max}^{\text{gen}} - \eta_{\max}}{\eta_{\max}}$ ) are given.

If we use the exact  $Z_{\text{gen}}, \tau, \beta$ , the standard error (=root mean square of relative errors) of  $\eta_{\max}^{\text{gen}}$  is  $9.60 \times 10^{-4}$ .

If we use  $Z_{\text{gen}}^{(0)}, \tau_{\text{lin}}^{(0)}, \beta_{\text{lin}}^{(0)}$ , the standard error is  $1.75 \times 10^{-2}$ . For the single crystalline SnSe with peak  $zT$  of 2.6, the relative error of one shot method is found to be only  $6.82 \times 10^{-3}$ . However, when we use the different approximation such as linear  $T(x)$  or different average scheme for  $z$ , the error becomes larger than ours due to the non-linearity of  $T$  for this material [269].

If we only use the  $Z_{\text{gen}}^{(0)}$  with zero  $\tau$  and  $\beta$ , the efficiency is still well predicted with the standard error of  $3.37 \times 10^{-2}$ . But, in some materials, the error is relatively large due to the neglect of the  $\tau$  and  $\beta$ . The largest relative error of 10% is found for [101], due to

TABLE S5. Statistics on the relative error (RelErr) of the maximum efficiency estimation formula  $\eta_{\max}^{\text{gen}}(Z_{\text{gen}}, \tau, \beta)$  in (15). Average (Avg), root mean square (RMS RelErr or StdErr), maximum (max), and minimum (min) of the relative errors are estimated for 276 materials for thermoelectric power generator working at their available temperature.

276 materials for power module	Relative error in maximum efficiency formula					
	$\eta_{\max}^{\text{gen}}$					$\eta_{\max}^{\text{const}}$
	$Z_{\text{gen}}, \tau, \beta$	$Z_{\text{gen}}^{(0)}, \tau^{(0)}, \beta^{(0)}$	$Z_{\text{gen}}^{(0)}, T_{\text{lin}}^{(0)}, \beta_{\text{lin}}^{(0)}$	$Z_{\text{gen}}$	$Z_{\text{gen}}^{(0)}$	peak $zT$
Avg RelErr	0.02%	1.11%	1.08%	1.42%	2.29%	235%
StdErr (RMS RelErr)	0.09%	1.38%	1.38%	1.52%	2.47%	1854%
max RelErr	1.15%	5.45%	5.23%	5.80%	9.96%	28835%
min RelErr	-0.61%	-1.92%	-1.76%	-1.78%	-2.48%	-4%

the non-vanishing gradient parameters ( $\tau = -0.222 \approx \tau^{(0)} = -0.177 \approx \tau_{\text{lin}}^{(0)} = -0.204$ ,  $\beta = 0.2085 \approx \beta^{(0)} = 0.228 \approx \beta_{\text{lin}}^{(0)} = 0.185$ , when  $T_h = 918K$  and  $T_c = 304K$ ).

## 12. EFFICIENCY RANK ESTIMATION USING $Z_{\text{gen}}^{(0)}$

The  $Z_{\text{gen}}$  is a figure of merit, so the bigger  $Z_{\text{gen}}$  usually implies the bigger maximum efficiency. Then if we rank TE devices in order of  $Z_{\text{gen}}$ , will we get the correct rank in order of exact maximum efficiency? To measure such an effect quantitatively, we define the *top-rank-preserving probability* by the ratio of the number of correct top ranks predicted by some estimation parameter, to the total number of top ranks.

In Table S6, we observe the top-rank-preserving probability is high even if we use the simplest estimation  $Z_{\text{gen}}^{(0)}$ . We computed the maximum thermoelectric efficiency of 5-stage segmented leg for all possible configuration using 18 candidates materials in Table S2. Thus there are  $18^5 = 1,889,568$  device structures. No contact resistance is imposed, but it can be easily imposed in our numerical schme by adding a stage with zero Seebeck coefficient. The result shows with the 82% probability, the top 1% rank configurations in order of exact maximum efficiency can be found in the top 1% ranks in order of  $Z_{\text{gen}}^{(0)}$ . Hence one may perform faster high-throughput screening by computing  $Z_{\text{gen}}^{(0)}$  only, without having to compute the numerical maximum efficiency.

*Additional information.* The best efficiency in the setting of Table S6 is 21.95% while the one-shot approximation  $\eta_{\max}^{\text{gen}}(Z_{\text{gen}}^{(0)}, \tau^{(0)}, \beta^{(0)})$  predicts it would be 22.30%. For top 100,000 configurations, the root mean square error is 0.0415.

*Computation algorithm.* The maximum thermoelectric conversion efficiency of a given device configuration is computed using the following procedures.

- (1) Prepare the thermoelectric property curves using digitized data. Each curve is linearly interpolated at intermediate temperature and extrapolated as constant values at the end point temperatures.
- (2) Choose the linear function as the initial guess  $T_0$  of exact temperature distribution.
- (3) Given a temperature distribution  $T_n$ , compute thermoelectric degrees of freedom using the definition in (3) and (12). Then estimate the optimal current density

TABLE S6. Comparison of top ranks in order of exact maximum efficiency and estimation parameters. The Top-rank-preserving probability means the ratio of the number of correct top ranks predicted by the estimation parameter, to the total number of top ranks. The 18 candidates materials in Table S2 are used to generate 5-stage segmented legs. Each stage of the leg has the same cross sectional area  $1\text{ mm}^2$  and the same length  $1/5\text{ mm}$  (total length is  $1\text{ mm}$ ). The hot- and cold-side temperatures are  $T_h = 900\text{K}$  and  $T_c = 300\text{K}$ .

Rank		Top-Rank-Preserving Probability		
		$Z_{\text{gen}}$	$\eta_{\text{max}}^{\text{gen}}(Z_{\text{gen}}^{(0)}, \tau^{(0)}, \beta^{(0)})$	$Z_{\text{gen}}^{(0)}$
Top 0.1%	<1,891	87%	73%	73%
Top 1%	<18,897	90%	84%	82%
Top 2%	<37,792	93%	88%	86%
Top 4%	<75,584	94%	89%	90%
All configurations	1,889,568	100%	100%	100%

$J$  using the formula (14). If a given structure is segmented, the material properties are position-dependent as well as temperature-dependent (but there is no additional difficulty in computation).

- (4) Compute  $T_{n+1}$  by evaluating the right-hand side of the integral equation (9).
- (5) If  $T_{n+1}$  agrees with  $T_n$ , go to the next step. Otherwise replace  $T_n$  by  $T_{n+1}$  and go back to the step 3.
- (6) Using the converged temperature distribution  $T_{n+1}$ , compute the maximum efficiency from  $\eta_{\text{max}}^{\text{gen}}(Z_{\text{gen}}, \tau, \beta)$ .

*Computation time.* In a single core computer, the computation of the maximum efficiency of a segmented leg takes less than 1 second. Thus, for total computation, it may take about 525 hours (22 days). We used a high-performance-computing (HPC) system consisting of 500 processors so the computation took about 1 hour.

### 13. WHY PEAK $zT$ FAILS FOR BiSbTe-LIKE AND SnSe-LIKE MATERIALS

While the peak  $zT$  of SnSe-like materials is significantly greater than that of BiSbTe-like materials, the efficiency of the latter is significantly greater than the former (SnSe has the highest peak  $zT$  of 2.6 at 923 K); see Figure 1 in the paper. This extreme failure case of  $zT$  can be explained by our additional figure of merit  $\tau$ .

Consider three imaginary materials imitating BiSbTe-like, SnSe-like, and constant- $z$  materials. For simplicity, we impose some assumptions on their material properties. The  $\rho$  and  $\kappa$  of them are temperature-independent and they have the same  $\bar{\alpha}$ . The  $\alpha$  of them is linear on temperature; the BiSbTe-like material has linearly decreasing  $\alpha$ , the SnSe-like material has linearly increasing  $\alpha$ , and the constant- $z$  material has the constant  $\alpha$ . Then, as shown in Figure S7, the peak  $zT$  of the SnSe-like material is very high. However, due to the temperature-dependent profile of  $\alpha$ , the  $\tau$  of the SnSe-like material is negative while the  $\tau$  of BiSbTe-like material is positive; see (18). Since the  $Z_{\text{gen}}$  is the same for the three materials, the  $\tau$  is the main figure of merit which concludes that the BiSbTe-like

material has higher maximum efficiency than the SnSe-like material. This example shows the gradient of material properties can affect the maximum efficiency.

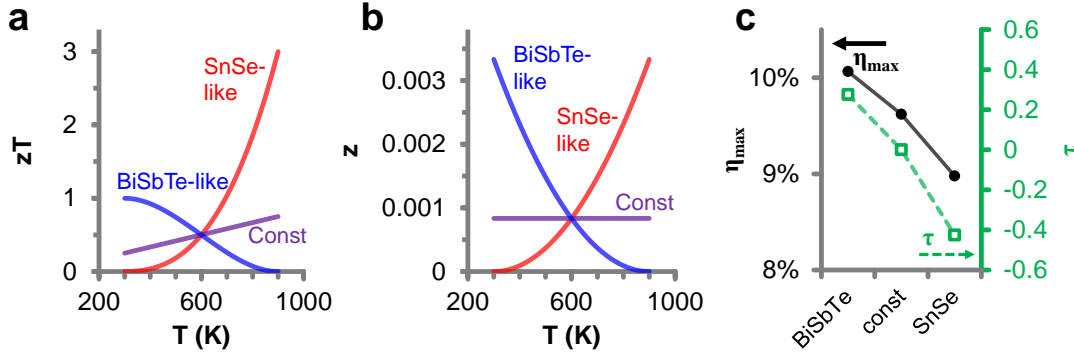


FIGURE S7. The  $zT$ , the maximum efficiency, and  $\tau$  for three imaginary materials which imitates BiSbTe-like, SnSe-like, and constant- $z$  materials. The  $\alpha$  of the materials is linear while the  $\rho$  and  $\kappa$  of them are constant. The materials have the same  $\bar{\alpha}$  and  $Z_{\text{gen}}$ . For working temperature from 300K to 900K, the highest maximum efficiency is found in the BiSbTe-like material due to the positive  $\tau$ .

#### 14. OPTIMAL DOPING CONCENTRATION FOR $\text{Bi}_2\text{Te}_3$

In this section, using *calculated* material properties, we design functionally graded materials (FGM) composed of  $\text{Bi}_2\text{Te}_3$  to maximize the efficiency. The thermoelectric properties are calculated using the density functional theory (DFT) [270, 271] combined with the Boltzmann transport equation. For the DFT calculations, we use the generalized gradient approximation (GGA) parameterized by PBE(Perdew, Burke, and Ernzerhof) [272], and the projector augmented-wave (PAW) pseudopotential [273]; both of them are implemented in the VASP code [274, 275]. The experimental lattice parameters for  $\text{Bi}_2\text{Te}_3$  are used, while the internal coordinates are fully relaxed. The electronic band structure is calculated using the spin-orbit interaction. The  $k$ -point mesh of  $36 \times 36 \times 36$  is used. The electronic transport properties are predicted using the DFT band structure coupled with the Boltzmann transport equation within a rigid band approximation and the constant relaxation time approximation; they are implemented in BoltzTraP code [276, 277]. Note that we use the experimental band gap of 0.18 eV. The phonon thermal conductivity is calculated using phono3py code [278, 279]. The force constants are obtained from the 240-atom supercell with the two-atom displacements using VASP code with the single  $k$ -point  $\Gamma$  and then the third-order phonon Hamiltonian is constructed. The three phonon scattering rates are calculated using the Fermi's golden rule. We also include the effective boundary scattering of 10 nm in addition to the three-phonon scattering. Then the thermal conductivity is calculated by integrating the conductivity on the phonon  $q$ -point mesh of  $11 \times 11 \times 11$ .

We calculate the maximum efficiency of functional gradient layers (FGL) based on  $\text{Bi}_2\text{Te}_3$  for temperature range from 300 K to 600 K. We consider various segmented

devices having 1 stage to 8 stages with eight different carrier concentrations ( $8 \times 10^{18}$ ,  $1 \times 10^{19}$ ,  $2 \times 10^{19}$ ,  $4 \times 10^{19}$ ,  $8 \times 10^{19}$ ,  $1 \times 10^{20}$ ,  $2 \times 10^{20}$   $\text{cm}^{-3}$ ). We perform high-throughput computation to find the optimal segmented FGL. There are  $8^8$  possible configurations in total. The temperature distribution inside a device is obtained by using fixed-point iteration of the integral equation (9). At the same time, the current density is optimized to find the maximum efficiency; see *Computation algorithm* in §12 for more details. Figure S8 shows the thermoelectric properties calculated by DFT, various segmented structures with its efficiency, and the optimal carrier concentration as a function of position. Figure S9 shows the highest efficiency is obtained for a 5-stage segmented device. For single stage, the maximum efficiency of 10.5 % is found at the doping concentration  $4 \times 10^{19}$   $\text{cm}^{-3}$ . For multi-stage, the maximum efficiency is found at the 5-stage with the optimal carrier concentration varying from  $8 \times 10^{19}$   $\text{cm}^{-3}$  to  $1 \times 10^{19}$   $\text{cm}^{-3}$  as going from hot to cold side.

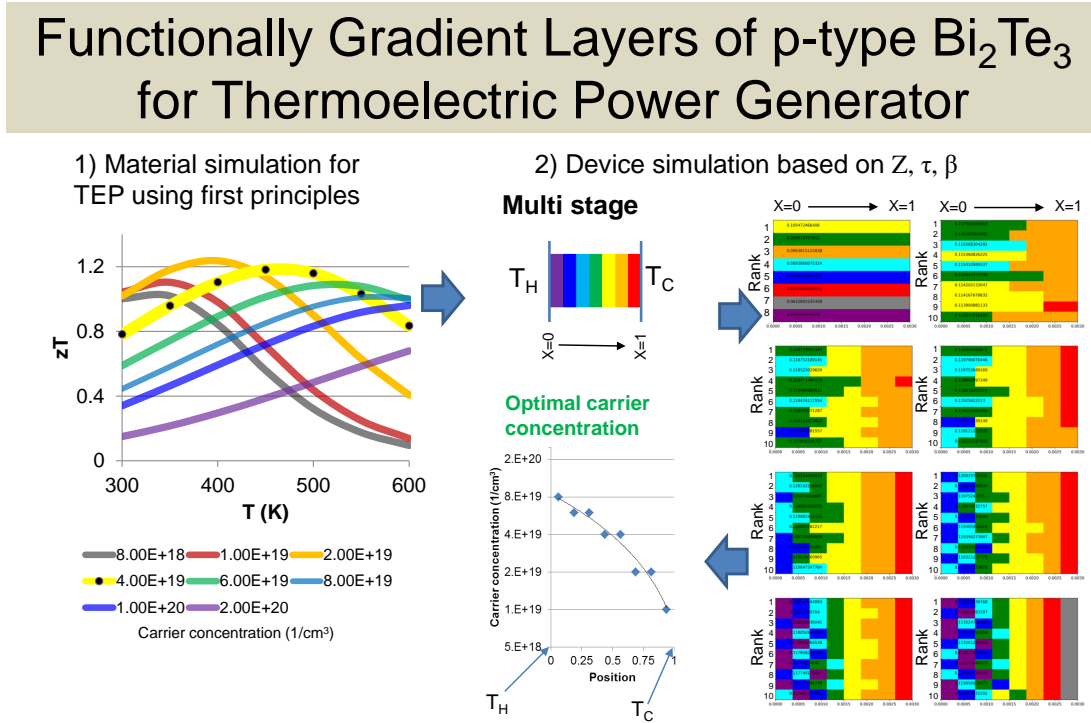


FIGURE S8. Design process of functionally graded materials for thermoelectric power generator and its result. The temperature range from 300 K to 600 K is considered. High-throughput computation of efficiency is performed to search the optimal carrier doping concentration. (Left) Thermoelectric properties of  $\text{Bi}_2\text{Te}_3$  calculated by DFT. (Middle top) Schematic structure of segmented devices; different color means different doping concentration. (Right) Top 10 segmented structures when the number of stage (number of segmentation of equal length) is fixed; 1 to 8 stages are considered. (Middle bottom) Optimal carrier doping concentration having the highest efficiency.

## Optimal segmentation for p-Bi<sub>2</sub>Te<sub>3</sub> leg

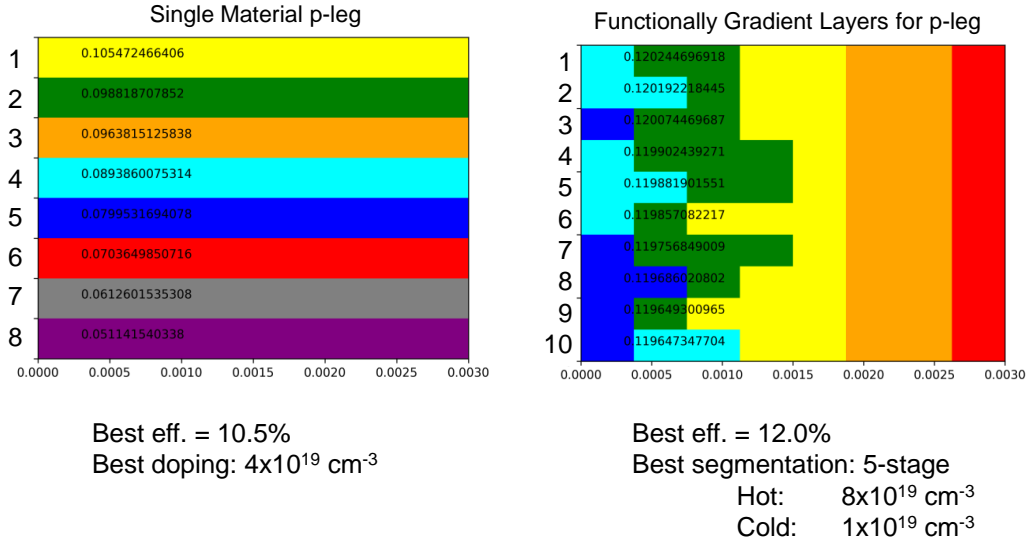


FIGURE S9. Top 10 segmented structures ranked in order of maximum efficiency. (Left) No segmentation. (Right) 5-stage segmentation. Each color represents a distinct material. The top rank structure is shown in the first row: yellow is the first rank for no segmentation. The 1cyan-2green-2yellow-2orange-1red segmented structure in the first row of the right figure is optimal among the 8<sup>8</sup> configurations with the highest efficiency of 12.0%.

### ACKNOWLEDGEMENT

This work was supported by Korea Electrotechnology Research Institute (KERI) Primary research program through the National Research Council of Science and Technology (NST) funded by the Ministry of Science and ICT (MSIT) of the Republic of Korea [No. 18-12-N0101-34 (Development of Design Tools of Thermoelectric and Energy Materials)]. This work was also supported by the Korea Institute of Energy Technology Evaluation and Planning (KETEP) and the Ministry of Trade, Industry and Energy (MOTIE) of the Republic of Korea [No. 20162000000910 (Development of High Performance Thermoelectric Modules by Power Modulation) and No. 20172010000830 (Developments of Thermoelectric Power Generation System using Unused Heats in Industry and Business Model)].

## REFERENCES

- [1] Biswas, K. *et al.* Strained endotaxial nanostructures with high thermoelectric figure of merit. *Nat Chem* **3**, 160–166 (2011).
- [2] Biswas, K. *et al.* High-performance bulk thermoelectrics with all-scale hierarchical architectures. *Nature* **489**, 414–418 (2012).
- [3] Fu, C. *et al.* Realizing high figure of merit in heavy-band *p*-type half-Heusler thermoelectric materials. *Nat Commun* **6**, 8144 (2015).
- [4] Gelbstein, Y., Davidow, J., Girard, S. N., Chung, D. Y. & Kanatzidis, M. Controlling metallurgical phase separation reactions of the  $\text{Ge}_{0.87}\text{Pb}_{0.13}\text{Te}$  alloy for high thermoelectric performance. *Adv. Energy Mater.* **3**, 815–820 (2013).
- [5] He, Y. *et al.* Ultrahigh thermoelectric performance in mosaic crystals. *Adv. Mater.* **27**, 3639–3644 (2015).
- [6] Heremans, J. P. *et al.* Enhancement of thermoelectric efficiency in PbTe by distortion of the electronic density of states. *Science* **321**, 554–557 (2008).
- [7] Hsu, K. F. *et al.* Cubic  $\text{AgPb}_m\text{SbTe}_{2+m}$ : Bulk thermoelectric materials with high figure of merit. *Science* **303**, 818–821 (2004).
- [8] Hu, L.-P. *et al.* Shifting up the optimum figure of merit of *p*-type bismuth telluride-based thermoelectric materials for power generation by suppressing intrinsic conduction. *NPG Asia Mater* **6**, e88 (2014).
- [9] Hu, X. *et al.* Power generation from nanostructured PbTe-based thermoelectrics: comprehensive development from materials to modules. *Energy Environ. Sci.* **9**, 517–529 (2016).
- [10] Kim, S. I. *et al.* Dense dislocation arrays embedded in grain boundaries for high-performance bulk thermoelectrics. *Science* **348**, 109–114 (2015).
- [11] Lin, S. *et al.* Tellurium as a high-performance elemental thermoelectric. *Nat Commun* **7**, 10287 (2016).
- [12] Liu, W.-S. *et al.* Thermoelectric property studies on Cu-doped *n*-type  $\text{Cu}_x\text{Bi}_2\text{Te}_{2.7}\text{Se}_{0.3}$  nanocomposites. *Advanced Energy Materials* **1**, 577–587 (2011).
- [13] Liu, W. *et al.* Convergence of conduction bands as a means of enhancing thermoelectric performance of *n*-type  $\text{Mg}_2\text{Si}_{1-x}\text{Sn}_x$  solid solutions. *Phys. Rev. Lett.* **108**, 166601 (2012).
- [14] Pan, Y. & Li, J.-F. Thermoelectric performance enhancement in *n*-type  $\text{Bi}_2(\text{TeSe})_3$  alloys owing to nanoscale inhomogeneity combined with a spark plasma-textured microstructure. *NPG Asia Mater* **8**, e275 (2016).
- [15] Pei, Y. *et al.* Convergence of electronic bands for high performance bulk thermoelectrics. *Nature* **473**, 66–69 (2011).
- [16] Pei, Y., LaLonde, A., Iwanaga, S. & Snyder, G. J. High thermoelectric figure of merit in heavy hole dominated PbTe. *Energy Environ. Sci.* **4**, 2085–2089 (2011).
- [17] Poudel, B. *et al.* High-thermoelectric performance of nanostructured bismuth antimony telluride bulk alloys. *Science* **320**, 634–638 (2008).
- [18] Rhyee, J.-S. *et al.* Peierls distortion as a route to high thermoelectric performance in  $\text{In}_4\text{Se}_{3-\delta}$  crystals. *Nature* **459**, 965–968 (2009).
- [19] Wang, H. *et al.* Right sizes of nano-and microstructures for high-performance and rigid bulk thermoelectrics. *Proceedings of the National Academy of Sciences* **111**, 10949–10954 (2014).
- [20] Zhao, L.-D. *et al.* Raising the thermoelectric performance of *p*-type PbS with endotaxial nanostructuring and valence-band offset engineering using CdS and ZnS. *J. Am. Chem. Soc.* **134**, 16327–16336 (2012).
- [21] Zhao, L.-D. *et al.* Thermoelectrics with earth abundant elements: High performance *p*-type PbS nanostructured with SrS and CaS. *J. Am. Chem. Soc.* **134**, 7902–7912 (2012).
- [22] Zhao, L.-D. *et al.* Ultralow thermal conductivity and high thermoelectric figure of merit in SnSe crystals. *Nature* **508**, 373–377 (2014).
- [23] Zhao, L.-D. *et al.* Ultrahigh power factor and thermoelectric performance in hole-doped single-crystal SnSe. *Science* aad3749 (2015).



- [24] Cui, J. L. *et al.* Thermoelectric properties of Ag-doped  $n$ -type  $(\text{Bi}_2\text{Te}_3)_{0.9}\text{-(Bi}_{2-x}\text{Ag}_x\text{Se}_3)_{0.1}$  ( $x=0\text{--}0.4$ ) alloys prepared by spark plasma sintering. *Journal of Solid State Chemistry* **180**, 1158–1162 (2007).
- [25] Cui, J. L. *et al.* Crystal structure analysis and thermoelectric properties of  $p$ -type pseudo-binary  $(\text{Al}_2\text{Te}_3)_x\text{-Bi}_{0.5}\text{Sb}_{1.5}\text{Te}_3)_{1-x}$  ( $x=0\text{--}0.2$ ) alloys prepared by spark plasma sintering. *Journal of Alloys and Compounds* **460**, 426–431 (2008).
- [26] Eum, A.-Y. *et al.* Transport and thermoelectric properties of  $\text{Bi}_2\text{Te}_{2.7}\text{Se}_{0.3}$  prepared by mechanical alloying and hot pressing. *Journal of the Korean Physical Society* **66**, 1726–1731 (2015).
- [27] Fan, S. *et al.*  $p$ -type  $\text{Bi}_{0.4}\text{Sb}_{1.6}\text{Te}_3$  nanocomposites with enhanced figure of merit. *Applied Physics Letters* **96**, 182104 (2010).
- [28] Han, M.-K., Kim, S., Kim, H.-Y. & Kim, S.-J. An alternative strategy to construct interfaces in bulk thermoelectric material: nanostructured heterophase  $\text{Bi}_2\text{Te}_3/\text{Bi}_2\text{S}_3$ . *RSC Adv.* **3**, 4673–4679 (2013).
- [29] HSU, H. C., HUANG, J.-Y. & HUANG, T.-K. Enhancing figure of merit of  $\text{Bi}_{0.5}\text{Sb}_{1.5}\text{Te}_3$  through nano-composite approach. *China Steel Technical Report* **27**, 57–63 (2014).
- [30] Zheng, Y. *et al.* Mechanically robust BiSbTe alloys with superior thermoelectric performance: A case study of stable hierarchical nanostructured thermoelectric materials. *Adv. Energy Mater.* **5**, 1401391 (2014).
- [31] Hu, L. *et al.* Tuning multiscale microstructures to enhance thermoelectric performance of  $n$ -type bismuth-telluride-based solid solutions. *Adv. Energy Mater.* **5**, 1500411 (2015).
- [32] Hwang, S. *et al.* Enhancing the thermoelectric properties of  $p$ -type bulk Bi-Sb-Te nanocomposites via solution-based metal nanoparticle decoration. *Journal of Elec Materi* **42**, 1411–1416 (2013).
- [33] Ko, J. *et al.* Nanograined thermoelectric  $\text{Bi}_2\text{Te}_{2.7}\text{Se}_{0.3}$  with ultralow phonon transport prepared from chemically exfoliated nanoplatelets. *Journal of Materials Chemistry A* **1**, 12791 (2013).
- [34] Zhang, Q. *et al.* Improved thermoelectric performance of silver nanoparticles-dispersed  $\text{Bi}_2\text{Te}_3$  composites deriving from hierarchical two-phased heterostructure. *Adv. Funct. Mater.* **25**, 966–976 (2015).
- [35] Zhao, X. B. *et al.* Bismuth telluride nanotubes and the effects on the thermoelectric properties of nanotube-containing nanocomposites. *Applied Physics Letters* **86**, 062111 (2005).
- [36] Lee, J. K. *et al.* Control of thermoelectric properties through the addition of Ag in the  $\text{Bi}_{0.5}\text{Sb}_{1.5}\text{Te}_3$  alloy. *Electron. Mater. Lett.* **6**, 201–207 (2010).
- [37] Lee, K.-H. *et al.* Enhancement of the thermoelectric performance of  $\text{Bi}_{0.4}\text{Sb}_{1.6}\text{Te}_3$  alloys by In and Ga doping. *Journal of Elec Materi* **42**, 1617–1621 (2013).
- [38] Lee, D. S. *et al.* Crystal structure, properties and nanostructuring of a new layered chalcogenide semiconductor,  $\text{Bi}_2\text{MnTe}_4$ . *CrystEngComm* **15**, 5532–5538 (2013).
- [39] Yan, X. *et al.* Experimental studies on anisotropic thermoelectric properties and structures of  $n$ -type  $\text{Bi}_2\text{Te}_{2.7}\text{Se}_{0.3}$ . *Nano Lett.* **10**, 3373–3378 (2010).
- [40] Lee, G.-E. *et al.* Preparation and thermoelectric properties of doped  $\text{Bi}_2\text{Te}_3\text{-Bi}_2\text{Se}_3$  solid solutions. *Journal of Elec Materi* **43**, 1650–1655 (2013).
- [41] Lee, G.-E. *et al.* Preparation and thermoelectric properties of  $\text{Bi}_2\text{Te}_3\text{-Bi}_2\text{Se}_3$  solid solutions. *Journal of the Korean Physical Society* **64**, 1416–1420 (2014).
- [42] Lee, G.-E. *et al.* Preparation and thermoelectric properties of iodine-doped  $\text{Bi}_2\text{Te}_3\text{-Bi}_2\text{Se}_3$  solid solutions. *Journal of the Korean Physical Society* **65**, 696–701 (2014).
- [43] Lee, G.-E. *et al.* Preparation and thermoelectric properties of  $n$ -type  $\text{Bi}_2\text{Te}_{2.7}\text{Se}_{0.3}\text{:Dm}$ . *Journal of Elec Materi* **44**, 1579–1584 (2014).
- [44] Lee, G.-E. *et al.* Thermoelectric properties of I-doped  $\text{Bi}_2\text{Te}_{2.85}\text{Se}_{0.15}$  solid solutions. *Journal of the Korean Physical Society* **64**, 1692–1696 (2014).
- [45] Sumithra, S. *et al.* Enhancement in thermoelectric figure of merit in nanostructured  $\text{Bi}_2\text{Te}_3$  with semimetal nano-inclusions. *Adv. Energy Mater.* **1**, 1141–1147 (2011).
- [46] Lukas, K. C., Liu, W. S., Ren, Z. F. & Opeil, C. P. Transport properties of Ni, Co, Fe, Mn doped  $\text{Cu}_{0.01}\text{Bi}_2\text{Te}_{2.7}\text{Se}_{0.3}$  for thermoelectric device applications. *Journal of Applied Physics* **112**, 054509 (2012).

- [47] Min, Y. *et al.* Surfactant-free scalable synthesis of  $\text{Bi}_2\text{Te}_3$  and  $\text{Bi}_2\text{Se}_3$  nanoflakes and enhanced thermoelectric properties of their nanocomposites. *Advanced Materials* **25**, 1425–1429 (2013).
- [48] Mun, H. *et al.* Fe-doping effect on thermoelectric properties of  $p$ -type  $\text{Bi}_{0.48}\text{Sb}_{1.52}\text{Te}_3$ . *Materials* **8**, 959–965 (2015).
- [49] Ovsyannikov, S. V. *et al.* Enhanced power factor and high-pressure effects in  $(\text{Bi},\text{Sb})_2(\text{Te},\text{Se})_3$  thermoelectrics. *Applied Physics Letters* **106**, 143901 (2015).
- [50] Puneet, P. *et al.* Preferential scattering by interfacial charged defects for enhanced thermoelectric performance in few-layered  $n$ -type  $\text{Bi}_2\text{Te}_3$ . *Sci. Rep.* **3** (2013).
- [51] Shin, H. S. *et al.* Twin-driven thermoelectric figure-of-merit enhancement of  $\text{Bi}_2\text{Te}_3$  nanowires. *Nanoscale* **6**, 6158 (2014).
- [52] Son, J. S. *et al.*  $n$ -type nanostructured thermoelectric materials prepared from chemically synthesized ultrathin  $\text{Bi}_2\text{Te}_3$  nanoplates. *Nano Lett.* **12**, 640–647 (2012).
- [53] Son, J. H. *et al.* Effect of ball milling time on the thermoelectric properties of  $p$ -type  $(\text{Bi},\text{Sb})_2\text{Te}_3$ . *Journal of Alloys and Compounds* **566**, 168–174 (2013).
- [54] Soni, A. *et al.* Enhanced thermoelectric properties of solution grown  $\text{Bi}_2\text{Te}_{3-x}\text{Se}_x$  nanoplatelet composites. *Nano Lett.* **12**, 1203–1209 (2012).
- [55] Xiao, Y. *et al.* Enhanced thermoelectric figure of merit in  $p$ -type  $\text{Bi}_{0.48}\text{Sb}_{1.52}\text{Te}_3$  alloy with  $\text{WSe}_2$  addition. *J. Mater. Chem. A* **2**, 8512–8516 (2014).
- [56] Tang, X. *et al.* Preparation and thermoelectric transport properties of high-performance  $p$ -type  $\text{Bi}_2\text{Te}_3$  with layered nanostructure. *Applied Physics Letters* **90**, 012102 (2007).
- [57] Wang, S., Li, H., Lu, R., Zheng, G. & Tang, X. Metal nanoparticle decorated  $n$ -type  $\text{Bi}_2\text{Te}_3$ -based materials with enhanced thermoelectric performances. *Nanotechnology* **24**, 285702 (2013).
- [58] Wu, F. *et al.* Thermoelectric properties of Ce-doped  $n$ -type  $\text{Ce}_x\text{Bi}_{2-x}\text{Te}_{2.7}\text{Se}_{0.3}$  nanocomposites. *Phys. Status Solidi A* **210**, 1183–1189 (2013).
- [59] Yelgel, Ö. C. & Srivastava, G. P. Thermoelectric properties of  $n$ -type  $\text{Bi}_2(\text{Te}_{0.85}\text{Se}_{0.15})_3$  single crystals doped with  $\text{CuBr}$  and  $\text{SbI}_3$ . *Phys. Rev. B* **85**, 125207 (2012).
- [60] Zhang, G. *et al.* Rational synthesis of ultrathin  $n$ -type  $\text{Bi}_2\text{Te}_3$  nanowires with enhanced thermoelectric properties. *Nano Lett.* **12**, 56–60 (2012).
- [61] Wei, P. *et al.* Minimum thermal conductivity in weak topological insulators with bismuth-based stack structure. *Adv. Funct. Mater.* **26**, 5360–5367 (2016).
- [62] Lan, J., Lin, Y.-H., Liu, Y., Xu, S. & Nan, C.-W. High thermoelectric performance of nanostructured  $\text{In}_2\text{O}_3$ -based ceramics. *Journal of the American Ceramic Society* **95**, 2465–2469 (2012).
- [63] Yu, C. *et al.* Preparation and thermoelectric properties of inhomogeneous bismuth telluride alloyed nanorods. *Journal of Alloys and Compounds* **570**, 86–93 (2013).
- [64] Kosuga, A. *et al.* Enhanced thermoelectric performance of In-substituted  $\text{GeSb}_6\text{Te}_{10}$  with homologous structure. *APL Materials* **2**, 086102 (2014).
- [65] Scheele, M. *et al.* Thermoelectric properties of lead chalcogenide core shell nanostructures. *ACS Nano* **5**, 8541–8551 (2011).
- [66] Ahn, K., Li, C., Uher, C. & Kanatzidis, M. G. Improvement in the thermoelectric figure of merit by  $\text{La}/\text{Ag}$  cosubstitution in  $\text{PbTe}$ . *Chemistry of Materials* **21**, 1361–1367 (2009).
- [67] Ahn, K. *et al.* Exploring resonance levels and nanostructuring in the  $\text{PbTe}$ - $\text{CdTe}$  system and enhancement of the thermoelectric figure of merit. *J. Am. Chem. Soc.* **132**, 5227–5235 (2010).
- [68] Ahn, K. *et al.* Enhanced thermoelectric properties of  $p$ -type nanostructured  $\text{PbTe}$ - $\text{MTe}$  ( $\text{M} = \text{Cd}, \text{Hg}$ ) materials. *Energy Environ. Sci.* **6**, 1529–1537 (2013).
- [69] Androulakis, J. *et al.* Thermoelectric enhancement in  $\text{PbTe}$  with  $\text{K}$  or  $\text{Na}$  codoping from tuning the interaction of the light- and heavy-hole valence bands. *Phys. Rev. B* **82**, 115209 (2010).
- [70] Androulakis, J., Lee, Y., Todorov, I., Chung, D.-Y. & Kanatzidis, M. High-temperature thermoelectric properties of  $n$ -type  $\text{PbSe}$  doped with  $\text{Ga}$ ,  $\text{In}$ , and  $\text{Pb}$ . *Physical Review B* **83** (2011).
- [71] Bali, A., Kim, I.-H., Rogl, P. & Mallik, R. C. Thermoelectric properties of two-phase  $\text{PbTe}$  with indium inclusions. *Journal of Electronic Materials* (2013).
- [72] Bali, A., Wang, H., Snyder, G. J. & Mallik, R. C. Thermoelectric properties of indium doped  $\text{PbTe}_{1-y}\text{Se}_y$  alloys. *Journal of Applied Physics* **116**, 033707 (2014).

- [73] Wu, D. *et al.* Superior thermoelectric performance in PbTe-PbS pseudo-binary: Extremely low thermal conductivity and modulated carrier. *Energy & Environmental Science* **8**, 2056 (2015).
- [74] Dong, Y., McGuire, M. A., Malik, A.-S. & DiSalvo, F. J. Transport properties of undoped and Br-doped PbTe sintered at high-temperature and pressure  $\geq 4.0$  GPa. *Journal of Solid State Chemistry* **182**, 2602–2607 (2009).
- [75] Dow, H. S. *et al.* Effect of Ag or Sb addition on the thermoelectric properties of PbTe. *Journal of Applied Physics* **108**, 113709 (2010).
- [76] Falkenbach, O., Hartung, D., Klar, P. J., Koch, G. & Schlecht, S. Thermoelectric properties of nanostructured bismuth-doped lead telluride  $\text{Bi}_x(\text{PbTe})_{1-x}$  prepared by co-ball-milling. *Journal of Electronic Materials* **43**, 1674–1680 (2014).
- [77] Fan, H. *et al.* Enhanced thermoelectric performance of PbSe co-doped with Ag and Sb. *Journal of Alloys and Compounds* **639**, 106–110 (2015).
- [78] Fang, H., Feng, T., Yang, H., Ruan, X. & Wu, Y. Synthesis and thermoelectric properties of compositional-modulated lead telluride bismuth telluride nanowire heterostructures. *Nano Letters* **13**, 2058–2063 (2013).
- [79] Jaworski, C. M. *et al.* Valence-band structure of highly efficient *p*-type thermoelectric PbTe-PbS alloys. *Phys. Rev. B* **87**, 045203 (2013).
- [80] Jian, Z. *et al.* Significant band engineering effect of YbTe for high performance thermoelectric PbTe. *J. Mater. Chem. C* **3**, 12410–12417 (2015).
- [81] Keiber, T., Bridges, F., Sales, B. & Wang, H. Complex role for thallium in PbTe:Tl from local probe studies. *Physical Review B* **87** (2013).
- [82] Kim, M.-S., Lee, W.-J., Cho, K.-H., Ahn, J.-P. & Sung, Y.-M. Spinodally decomposed PbSe-PbTe nanoparticles for high-performance thermoelectrics: Enhanced phonon scattering and unusual transport behavior. *ACS Nano* **10**, 7197–7207 (2016).
- [83] Lee, J. K. *et al.* Improvement of thermoelectric properties through controlling the carrier concentration of  $\text{AgPb}_{18}\text{SbTe}_{20}$  alloys by Sb addition. *Electron. Mater. Lett.* **8**, 659–663 (2012).
- [84] Lee, Y. *et al.* Contrasting role of antimony and bismuth dopants on the thermoelectric performance of lead selenide. *Nat Commun* **5** (2014).
- [85] Li, X. *et al.* Enhanced thermoelectric properties of  $(\text{PbTe})_{0.88}(\text{PbS})_{0.12}$  composites by Bi doping. *Journal of Alloys and Compounds* **547**, 86–90 (2013).
- [86] Li, Z.-Y. *et al.* PbTe-based thermoelectric nanocomposites with reduced thermal conductivity by SiC nanodispersion. *Applied Physics Letters* **104**, 113905 (2014).
- [87] Liu, J., Wang, X. & Peng, L. Effect of annealing on thermoelectric properties of eutectic  $\text{PbTeSb}_2\text{Te}_3$  composite with self-assembled lamellar structure. *Intermetallics* **41**, 63–69 (2013).
- [88] Lo, S.-H., He, J., Biswas, K., Kanatzidis, M. G. & Dravid, V. P. Phonon scattering and thermal conductivity in *p*-type nanostructured PbTe-BaTe Bulk thermoelectric materials. *Adv. Funct. Mater.* **22**, 5175–5184 (2012).
- [89] Lu, P.-X., Qu, L.-B. & Cheng, Q.-H. Enhancement of thermoelectric figure of merit in binary-phased  $\text{La}_{0.3}\text{Ce}_{0.37}\text{Fe}_3\text{CoS}_{12}$ -PbTe materials. *Journal of Alloys and Compounds* **558**, 50–55 (2013).
- [90] Pei, Y., Heinz, N. A., LaLonde, A. & Snyder, G. J. Combination of large nanostructures and complex band structure for high performance thermoelectric lead telluride. *Energy Environ. Sci.* **4**, 3640–3645 (2011).
- [91] Pei, Y., Lensch-Falk, J., Toberer, E. S., Medlin, D. L. & Snyder, G. J. High thermoelectric performance in PbTe due to large nanoscale  $\text{Ag}_2\text{Te}$  precipitates and La doping. *Advanced Functional Materials* **21**, 241–249 (2011).
- [92] Pei, Y., May, A. F. & Snyder, G. J. Self-tuning the carrier concentration of PbTe/ $\text{Ag}_2\text{Te}$  composites with excess Ag for high thermoelectric performance. *Advanced Energy Materials* **1**, 291–296 (2011).
- [93] Pei, Y. *et al.* Stabilizing the optimal carrier concentration for high thermoelectric efficiency. *Adv. Mater.* **23**, 5674–5678 (2011).
- [94] Pei, Y., LaLonde, A. D., Wang, H. & Snyder, G. J. Low effective mass leading to high thermoelectric performance. *Energy Environ. Sci.* **5**, 7963–7969 (2012).

- [95] Pei, Y., Wang, H., Gibbs, Z. M., LaLonde, A. D. & Snyder, G. J. Thermopower enhancement in  $\text{Pb}_{1-x}\text{Mn}_x\text{Te}$  alloys and its effect on thermoelectric efficiency. *NPG Asia Mater* **4**, e28 (2012).
- [96] Pei, Y. *et al.* Optimum carrier concentration in  $n$ -type  $\text{PbTe}$  thermoelectrics. *Adv. Energy Mater.* **4**, 1400486 (2014).
- [97] Poudeu, P. F. P. *et al.* High thermoelectric figure of merit and nanostructuring in bulk  $p$ -type  $\text{Na}_{1-x}\text{Pb}_m\text{Sb}_y\text{Te}_{m+2}$ . *Angewandte Chemie International Edition* **45**, 3835–3839 (2006).
- [98] Rawat, P. K., Paul, B. & Banerji, P. Thermoelectric properties of  $\text{PbSe}_{0.5}\text{Te}_{0.5:x}(\text{PbI}_2)$  with endotaxial nanostructures: a promising  $n$ -type thermoelectric material. *Nanotechnology* **24**, 215401 (2013).
- [99] Wang, H. *et al.* Large enhancement in the thermoelectric properties of  $\text{Pb}_{0.98}\text{Na}_{0.02}\text{Te}$  by optimizing the synthesis conditions. *Journal of Materials Chemistry A* **1**, 11269 (2013).
- [100] Wang, H., Gibbs, Z. M., Takagiwa, Y. & Snyder, G. J. Tuning bands of  $\text{PbSe}$  for better thermoelectric efficiency. *Energy Environ. Sci.* **7**, 804–811 (2014).
- [101] Wu, H. J. *et al.* Broad temperature plateau for thermoelectric figure of merit  $ZT > 2$  in phase-separated  $\text{PbTe}_{0.7}\text{S}_{0.3}$ . *Nat Commun* **5**, 4515 (2014).
- [102] Wu, H. *et al.* Strong enhancement of phonon scattering through nanoscale grains in lead sulfide thermoelectrics. *NPG Asia Mater* **6**, e108 (2014).
- [103] Yamini, S. A. *et al.* Heterogeneous distribution of sodium for high thermoelectric performance of  $p$ -type multiphase lead-chalcogenides. *Adv. Energy Mater.* **5**, 1501047 (2015).
- [104] Yang, H. *et al.* Enhanced thermoelectric properties in bulk nanowire heterostructure-based nanocomposites through minority carrier blocking. *Nano Lett.* **15**, 1349 (2015).
- [105] Zebarjadi, M. *et al.* Power factor enhancement by modulation doping in bulk nanocomposites. *Nano Lett.* **11**, 2225–2230 (2011).
- [106] Zhang, Q. *et al.* Enhancement of thermoelectric figure-of-merit by resonant states of aluminium doping in lead selenide. *Energy & Environmental Science* **5**, 5246 (2012).
- [107] Zhang, Q. *et al.* Heavy doping and band engineering by potassium to improve the thermoelectric figure of merit in  $p$ -type  $\text{PbTe}$ ,  $\text{PbSe}$ , and  $\text{PbTe}_{1-y}\text{Se}_y$ . *J. Am. Chem. Soc.* **134**, 10031–10038 (2012).
- [108] Zhang, Q. *et al.* Effect of aluminum on the thermoelectric properties of nanostructured  $\text{PbTe}$ . *Nanotechnology* **24**, 345705 (2013).
- [109] Zhang, Q. *et al.* Enhancement of thermoelectric performance of  $n$ -type  $\text{PbSe}$  by Cr doping with optimized carrier concentration. *Adv. Energy Mater.* **5**, 1401977 (2015).
- [110] Al Rahal Al Orabi, R. *et al.* Band degeneracy, low thermal conductivity, and high thermoelectric figure of merit in  $\text{SnTe-CaTe}$  alloys. *Chem. Mater.* **28**, 376–384 (2015).
- [111] Banik, A., Shenoy, U. S., Anand, S., Waghmare, U. V. & Biswas, K. Mg alloying in  $\text{SnTe}$  facilitates valence band convergence and optimizes thermoelectric properties. *Chem. Mater.* **27**, 581–587 (2015).
- [112] Banik, A., Shenoy, U. S., Saha, S., Waghmare, U. V. & Biswas, K. High power factor and enhanced thermoelectric performance of  $\text{SnTe-AgInTe}_2$ : Synergistic effect of resonance level and valence band convergence. *Journal of the American Chemical Society* **138**, 13068–13075 (2016).
- [113] Banik, A. & Biswas, K. AgI alloying in  $\text{SnTe}$  boosts the thermoelectric performance via simultaneous valence band convergence and carrier concentration optimization. *Journal of Solid State Chemistry* **242**, 43–49 (2016).
- [114] Chen, C.-L., Wang, H., Chen, Y.-Y., Day, T. & Snyder, J. Thermoelectric properties of  $p$ -type polycrystalline  $\text{SnSe}$  doped with Ag. *J. Mater. Chem. A* **2**, 11171–11176 (2014).
- [115] Chen, Y.-X. *et al.* Understanding of the extremely low thermal conductivity in high-performance polycrystalline  $\text{SnSe}$  through potassium doping. *Adv. Funct. Mater.* **26**, 6836–6845 (2016).
- [116] Leng, H.-Q., Zhou, M., Zhao, J., Han, Y.-M. & Li, L.-F. The thermoelectric performance of anisotropic  $\text{SnSe}$  doped with Na. *RSC Adv.* **6**, 9112–9116 (2016).
- [117] Pei, Y. *et al.* Interstitial point defect scattering contributing to high thermoelectric performance in  $\text{SnTe}$ . *Adv. Electron. Mater.* **2**, 1600019 (2016).

- [118] Tan, G. *et al.* High thermoelectric performance of *p*-type SnTe via a synergistic band engineering and nanostructuring approach. *J. Am. Chem. Soc.* **136**, 7006–7017 (2014).
- [119] Tan, G. *et al.* Codoping in SnTe: Enhancement of thermoelectric performance through synergy of resonance levels and band convergence. *J. Am. Chem. Soc.* **137**, 5100–5112 (2015).
- [120] Tan, G. *et al.* Valence band modification and high thermoelectric performance in SnTe heavily alloyed with MnTe. *J. Am. Chem. Soc.* **137**, 11507–11516 (2015).
- [121] Tang, G. *et al.* Realizing high figure of merit in phase-separated polycrystalline  $\text{Sn}_{1-x}\text{Pb}_x\text{Se}$ . *Journal of the American Chemical Society* **138**, 13647–13654 (2016).
- [122] WANG, X. *et al.* Thermoelectric properties of Eu- and Na-substituted SnTe. *Journal of Rare Earths* **33**, 1175–1181 (2015).
- [123] Zhang, Q. *et al.* High thermoelectric performance by resonant dopant indium in nanostructured SnTe. *Proceedings of the National Academy of Sciences* **110**, 13261–13266 (2013).
- [124] Zhou, M. *et al.* Optimization of thermoelectric efficiency in SnTe: the case for the light band. *Phys. Chem. Chem. Phys.* **16**, 20741–20748 (2014).
- [125] Guan, X. *et al.* Thermoelectric properties of SnSe compound. *Journal of Alloys and Compounds* **643**, 116–120 (2015).
- [126] Suzuki, Y. & Nakamura, H. A supercell approach to the doping effect on the thermoelectric properties of SnSe. *Phys. Chem. Chem. Phys.* **17**, 29647–29654 (2015).
- [127] Fahrnbauer, F., Souchay, D., Wagner, G. & Oeckler, O. High thermoelectric figure of merit values of germanium antimony tellurides with kinetically stable cobalt germanide precipitates. *J. Am. Chem. Soc.* **137**, 12633–12638 (2015).
- [128] Gelbstein, Y., Dashevsky, Z. & Dariel, M. In-doped  $\text{Pb}_{0.5}\text{Sn}_{0.5}\text{Te}$  *p*-type samples prepared by powder metallurgical processing for thermoelectric applications. *Physica B: Condensed Matter* **396**, 16–21 (2007).
- [129] Gelbstein, Y., Dashevsky, Z. & Dariel, M. Powder metallurgical processing of functionally graded *p*- $\text{Pb}_{1-x}\text{Sn}_x\text{Te}$  materials for thermoelectric applications. *Physica B: Condensed Matter* **391**, 256–265 (2007).
- [130] Gelbstein, Y., Rosenberg, Y., Sadia, Y. & Dariel, M. P. Thermoelectric properties evolution of spark plasma sintered ( $\text{Ge}_{0.6}\text{Pb}_{0.3}\text{Sn}_{0.1}$ )Te following a spinodal decomposition. *The Journal of Physical Chemistry C* **114**, 13126–13131 (2010).
- [131] Hazan, E. *et al.* Effective electronic mechanisms for optimizing the thermoelectric properties of GeTe-rich alloys. *Adv. Electron. Mater.* **1**, 1500228 (2015).
- [132] Kusz, B., Miruszewski, T., Bochentyn, B., Lapiński, M. & Karczewski, J. Structure and thermoelectric properties of Te-Ag-Ge-Sb (TAGS) materials obtained by reduction of melted oxide substrates. *Journal of Elec Materi* **45**, 1085–1093 (2016).
- [133] Lee, J. K. *et al.* Influence of Mn on crystal structure and thermoelectric properties of GeTe compounds. *Electron. Mater. Lett.* **10**, 813–817 (2014).
- [134] Schroder, T. *et al.* Nanostructures in Te/Sb/Ge/Ag (TAGS) thermoelectric materials induced by phase transitions associated with vacancy ordering. *Inorg. Chem.* **53**, 7722–7729 (2014).
- [135] Schröder, T. *et al.* TAGS-related indium compounds and their thermoelectric properties—the solid solution series  $(\text{GeTe})_x\text{AgIn}_y\text{Sb}_{1-y}\text{Te}_2$  ( $x = 1-2$ ;  $y = 0.5$  and  $1$ ). *J. Mater. Chem. A* **2**, 6384–6395 (2014).
- [136] Williams, J. B., Lara-Curzio, E., Cakmak, E., Watkins, T. & Morelli, D. T. Enhanced thermoelectric performance driven by high-temperature phase transition in the phase change material  $\text{Ge}_4\text{SbTe}_5$ . *Journal of Materials Research FirstView*, 1–6 (2015).
- [137] Wu, D. *et al.* Origin of the high performance in GeTe-based thermoelectric materials upon  $\text{Bi}_2\text{Te}_3$  doping. *J. Am. Chem. Soc.* **136**, 11412–11419 (2014).
- [138] Aikebaier, Y., Kurosaki, K., Muta, H. & Yamanaka, S. Effect of (Pb,Ge)Te addition on the phase stability and the thermoelectric properties of  $\text{AgSbTe}_2$ . *MRS Online Proceedings Library* **1267**, 1267–DD04–11 (2010).
- [139] Chen, Y., He, B., Zhu, T. J. & Zhao, X. B. Thermoelectric properties of non-stoichiometric  $\text{AgSbTe}_2$  based alloys with a small amount of GeTe addition. *J. Phys. D: Appl. Phys.* **45**, 115302 (2012).

- [140] Dow, H. S. *et al.* Thermoelectric properties of  $\text{AgPb}_m\text{SbTe}_{m+2}$  ( $12 \leq m \leq 26$ ) at elevated temperature. *Journal of Applied Physics* **105**, 113703 (2009).
- [141] Drymiotis, F., Day, T. W., Brown, D. R., Heinz, N. A. & Snyder, G. J. Enhanced thermoelectric performance in the very low thermal conductivity  $\text{Ag}_2\text{Se}_{0.5}\text{Te}_{0.5}$ . *Applied Physics Letters* **103**, 143906 (2013).
- [142] Du, B., Li, H. & Tang, X. Effect of Ce substitution for Sb on the thermoelectric properties of  $\text{AgSbTe}_2$  compound. *Journal of Electronic Materials* **43**, 2384–2389 (2014).
- [143] Guin, S. N. & Biswas, K. Sb deficiencies control hole transport and boost the thermoelectric performance of *p*-type  $\text{AgSbSe}_2$ . *J. Mater. Chem. C* **3**, 10415–10421 (2015).
- [144] Han, M.-K., Androulakis, J., Kim, S.-J. & Kanatzidis, M. G. Lead-free thermoelectrics: High figure of merit in *p*-type  $\text{AgSn}_m\text{SbTe}_{m+2}$ . *Adv. Energy Mater.* **2**, 157–161 (2012).
- [145] He, Z. *et al.* Synthesis and thermoelectric properties of Mn-doped  $\text{AgSbTe}_2$  compounds. *Chinese Phys. B* **21**, 106101 (2012).
- [146] Hong, A. J. *et al.* Anomalous transport and thermoelectric performances of  $\text{CuAgSe}$  compounds. *Solid State Ionics* **261**, 21–25 (2014).
- [147] Liu, X., Jin, D. & Liang, X. Enhanced thermoelectric performance of *n*-type transformable  $\text{AgBiSe}_2$  polymorphs by indium doping. *Applied Physics Letters* **109**, 133901 (2016).
- [148] Mohanraman, R. *et al.* Influence of nanoscale  $\text{Ag}_2\text{Te}$  precipitates on the thermoelectric properties of the Sn doped *P*-type  $\text{AgSbTe}_2$  compound. *APL Materials* **2**, 096114 (2014).
- [149] Pei, Y., Heinz, N. A. & Snyder, G. J. Alloying to increase the band gap for improving thermoelectric properties of  $\text{Ag}_2\text{Te}$ . *J. Mater. Chem.* **21**, 18256–18260 (2011).
- [150] Wang, H., Li, J.-F., Zou, M. & Sui, T. Synthesis and transport property of  $\text{AgSbTe}_2$  as a promising thermoelectric compound. *Applied Physics Letters* **93**, 202106 (2008).
- [151] Wu, H.-j. *et al.* State of the art  $\text{Ag}_{50-x}\text{Sb}_x\text{Se}_{50-y}\text{Te}_y$  alloys: Their high  $zT$  values, microstructures and related phase equilibria. *Acta Materialia* **93**, 38–45 (2015).
- [152] Zhang, S. N., Zhu, T. J., Yang, S. H., Yu, C. & Zhao, X. B. Improved thermoelectric properties of  $\text{AgSbTe}_2$  based compounds with nanoscale  $\text{Ag}_2\text{Te}$  in situ precipitates. *Journal of Alloys and Compounds* **499**, 215–220 (2010).
- [153] Aizawa, T., Song, R. & Yamamoto, A. Solid state synthesis of ternary thermoelectric magnesium alloy. *Materials Transactions* **47**, 1058–1065 (2006).
- [154] Akasaka, M., Iida, T., Nishio, K. & Takahashi, Y. Composition dependent thermoelectric properties of sintered  $\text{Mg}_2\text{Si}_{1-x}\text{Ge}_x$  ( $x=0$  to 1) initiated from a melt-grown polycrystalline source. *Thin Solid Films* **515**, 8237–8241 (2007).
- [155] Akasaka, M. *et al.* Non-wetting crystal growth of  $\text{Mg}_2\text{Si}$  by vertical Bridgman method and thermoelectric characteristics. *Journal of Crystal Growth* **304**, 196–201 (2007).
- [156] Cheng, X., Farahi, N. & Kleinke, H.  $\text{Mg}_2\text{Si}$ -based materials for the thermoelectric energy conversion. *JOM* **68**, 2680–2687 (2016).
- [157] Duan, X., Hu, K., Kuang, J., Jiang, Y. & Yi, D. Effects of Ag-doping on thermoelectric properties of  $\text{Ca}_{(2-x)}\text{Ag}_x\text{Si}$  alloys. *Journal of Electronic Materials* **46**, 2986–2989 (2016).
- [158] Isoda, Y., Nagai, T., Fujiu, H., Imai, Y. & Shinohara, Y. The effect of Bi doping on thermoelectric properties of  $\text{Mg}_2\text{Si}_{0.5}\text{Sn}_{0.5}$ . In *2007 26th International Conference on Thermoelectrics*, 251–255 (2007).
- [159] Kajikawa, T. *et al.* Thermoelectric figure of merit of impurity doped and hot-pressed magnesium silicide elements. In *Seventeenth International Conference on Thermoelectrics. Proceedings ICT98 (Cat. No.98TH8365)*, 362–369 (1998).
- [160] Liu, W. *et al.* *n*-type thermoelectric material  $\text{Mg}_2\text{Sn}_{0.75}\text{Ge}_{0.25}$  for high power generation. *PNAS* **112**, 3269–3274 (2015).
- [161] Luo, W. *et al.* Fabrication and thermoelectric properties of  $\text{Mg}_2\text{Si}_{1-x}\text{Sn}_x$  solid solutions by solid state reaction and spark plasma sintering. *Materials Science and Engineering: B* **157**, 96–100 (2009).

- [162] Mars, K., Ihou-Mouko, H., Pont, G., Tobola, J. & Scherrer, H. Thermoelectric properties and electronic structure of Bi- and Ag-doped  $\text{Mg}_2\text{Si}_{1-x}\text{Ge}_x$  compounds. *Journal of Electronic Materials* **38**, 1360–1364 (2009).
- [163] Noda, Y., Kon, H., Furukawa, Y., Nishida, I. A. & Masumoto, K. Temperature dependence of thermoelectric properties of  $\text{Mg}_2\text{Si}_{0.6}\text{Ge}_{0.4}$ . *Mater. Trans., JIM* **33**, 851–855 (1992).
- [164] Tani, J.-i. & Kido, H. Thermoelectric properties of Bi-doped  $\text{Mg}_2\text{Si}$  semiconductors. *Physica B: Condensed Matter* **364**, 218–224 (2005).
- [165] Tani, J.-i. & Kido, H. Thermoelectric properties of P-doped  $\text{Mg}_2\text{Si}$  semiconductors. *Japanese Journal of Applied Physics* **46**, 3309–3314 (2007).
- [166] Tani, J.-i. & Kido, H. Thermoelectric properties of Sb-doped  $\text{Mg}_2\text{Si}$  semiconductors. *Intermetallics* **15**, 1202–1207 (2007).
- [167] Yang, M. J., Luo, W. J., Shen, Q., Jiang, H. Y. & Zhang, L. M. Preparation and thermoelectric properties of Bi-doped  $\text{Mg}_2\text{Si}$  nanocomposites. *Advanced Materials Research* **66**, 17–20 (2009).
- [168] Yin, K. *et al.* Optimization of the electronic band structure and the lattice thermal conductivity of solid solutions according to simple calculations: a canonical example of the  $\text{Mg}_2\text{Si}_{1-x-y}\text{Ge}_x\text{Sn}_y$  ternary solid solution. *Chemistry of Materials* **28**, 5538–5548 (2016).
- [169] Zhang, Q. *et al.* High figures of merit and natural nanostructures in  $\text{Mg}_2\text{Si}_{0.4}\text{Sn}_{0.6}$  based thermoelectric materials. *Applied Physics Letters* **93**, 102109 (2008).
- [170] Zhang, Q. *et al.* *In situ* synthesis and thermoelectric properties of La-doped  $\text{Mg}_2(\text{Si}, \text{Sn})$  composites. *Journal of Physics D: Applied Physics* **41**, 185103 (2008).
- [171] Zhang, L. *et al.* Suppressing the bipolar contribution to the thermoelectric properties of  $\text{Mg}_2\text{Si}_{0.4}\text{Sn}_{0.6}$  by Ge substitution. *Journal of Applied Physics* **117**, 155103 (2015).
- [172] Zhao, X. B. *et al.* Synthesis of nanocomposites with improved thermoelectric properties. *Journal of Electronic Materials* **38**, 1017–1024 (2009).
- [173] Joshi, G. *et al.* Enhanced thermoelectric figure-of-merit in nanostructured *p*-type silicon germanium bulk alloys. *Nano Lett.* **8**, 4670–4674 (2008).
- [174] Tang, J. *et al.* Holey silicon as an efficient thermoelectric material. *Nano Letters* **10**, 4279–4283 (2010).
- [175] Wang, X. W. *et al.* Enhanced thermoelectric figure of merit in nanostructured *n*-type silicon germanium bulk alloy. *Applied Physics Letters* **93**, 193121 (2008).
- [176] Ahn, K. *et al.* Improvement in the thermoelectric performance of the crystals of halogen-substituted  $\text{In}_4\text{Se}_{3-x}\text{H}_{0.03}$  ( $\text{H} = \text{F}, \text{Cl}, \text{Br}, \text{I}$ ): Effect of halogen-substitution on the thermoelectric properties in  $\text{In}_4\text{Se}_3$ . *J. Mater. Chem.* **22**, 5730–5736 (2012).
- [177] Bhatt, R. *et al.* Thermoelectric performance of layered  $\text{Sr}_x\text{TiSe}_2$  above 300 K. *J. Phys.: Condens. Matter* **26**, 445002 (2014).
- [178] Fu, C., Zhu, T., Liu, Y., Xie, H. & Zhao, X. Band engineering of high performance *p*-type FeNbSb based half-Heusler thermoelectric materials for figure of merit  $zT > 1$ . *Energy & Environmental Science* **8**, 216–220 (2015).
- [179] Kraemer, D. *et al.* High thermoelectric conversion efficiency of  $\text{MgAgSb}$ -based material with hot-pressed contacts. *Energy Environ. Sci.* **8**, 1299–1308 (2015).
- [180] Krez, J. *et al.* Long-term stability of phase-separated half-Heusler compounds. *Phys. Chem. Chem. Phys.* **17**, 29854–29858 (2015).
- [181] Liu, W.-S., Zhang, B.-P., Li, J.-F. & Zhao, L.-D. Thermoelectric property of fine-grained  $\text{CoSb}_3$  skutterudite compound fabricated by mechanical alloying and spark plasma sintering. *J. Phys. D: Appl. Phys.* **40**, 566 (2007).
- [182] Mudryk, Y. *et al.* Thermoelectricity of clathrate I Si and Ge phases. *J. Phys.: Condens. Matter* **14**, 7991 (2002).
- [183] Shi, X. *et al.* Low thermal conductivity and high thermoelectric figure of merit in *n*-type  $\text{Ba}_x\text{Yb}_y\text{Co}_4\text{Sb}_{12}$  double-filled skutterudites. *Applied Physics Letters* **92**, 182101 (2008).
- [184] Bai, S. *et al.* Enhanced thermoelectric performance of dual-element-filled skutterudites  $\text{Ba}_x\text{Ce}_y\text{Co}_4\text{Sb}_{12}$ . *Acta Materialia* **57**, 3135–3139 (2009).

- [185] Bao, S., Yang, J., Zhu, W., Fan, X. & Duan, X. Effect of processing parameters on formation and thermoelectric properties of  $\text{La}_{0.4}\text{FeCo}_3\text{Sb}_{12}$  skutterudite by MA-HP method. *Journal of Alloys and Compounds* **476**, 802–806 (2009).
- [186] Chitroub, M., Besse, F. & Scherrer, H. Thermoelectric properties of semi-conducting compound  $\text{CoSb}_3$  doped with Pd and Te. *Journal of Alloys and Compounds* **467**, 31–34 (2009).
- [187] Dong, N. *et al.* HPHT synthesis and thermoelectric properties of  $\text{CoSb}_3$  and  $\text{Fe}_{0.6}\text{Co}_{3.4}\text{Sb}_{12}$  skutterudites. *Journal of Alloys and Compounds* **480**, 882–884 (2009).
- [188] Duan, B., Zhai, P., Liu, L., Zhang, Q. & Ruan, X. Synthesis and high temperature transport properties of Te-doped skutterudite compounds. *Journal of Materials Science: Materials in Electronics* **23**, 1817–1822 (2012).
- [189] Dyck, J. S. *et al.* Thermoelectric properties of the *n*-type filled skutterudite  $\text{Ba}_{0.3}\text{Co}_4\text{Sb}_{12}$  doped with Ni. *Journal of Applied Physics* **91**, 3698–3705 (2002).
- [190] He, Z. *et al.* Thermoelectric properties of hot-pressed skutterudite  $\text{CoSb}_3$ . *Journal of Applied Physics* **101**, 053713 (2007).
- [191] He, Q. *et al.* The great improvement effect of pores on *ZT* in  $\text{Co}_{1-x}\text{Ni}_x\text{Sb}_3$  system. *Applied Physics Letters* **93**, 042108 (2008).
- [192] Laufek, F., Navratil, J., Plášil, J., Plecháček, T. & Drašar, Č. Synthesis, crystal structure and transport properties of skutterudite-related  $\text{CoSn}_{1.5}\text{Se}_{1.5}$ . *Journal of Alloys and Compounds* **479**, 102–106 (2009).
- [193] Li, X. Y. *et al.* Thermoelectric properties of Te-doped  $\text{CoSb}_3$  by spark plasma sintering. *Journal of Applied Physics* **98**, 083702 (2005).
- [194] Liang, T. *et al.* Ultra-fast synthesis and thermoelectric properties of Te doped skutterudites. *J. Mater. Chem. A* **2**, 17914–17918 (2014).
- [195] Liu, W.-S., Zhang, B.-P., Li, J.-F., Zhang, H.-L. & Zhao, L.-D. Enhanced thermoelectric properties in  $\text{CoSb}_{3-x}\text{Te}_x$  alloys prepared by mechanical alloying and spark plasma sintering. *Journal of Applied Physics* **102**, 103717 (2007).
- [196] Mallik, R. C. Transport properties of Sn-filled and Te-doped  $\text{CoSb}_3$  skutterudites. *Metals and Materials International* **14**, 615–620 (2008).
- [197] Mallik, R. C. *et al.* Thermoelectric properties of  $\text{Fe}_{0.2}\text{Co}_{3.8}\text{Sb}_{12-x}\text{Te}_x$  skutterudites. *Acta Materialia* **61**, 6698–6711 (2013).
- [198] Mi, J. L., Zhao, X. B., Zhu, T. J. & Tu, J. P. Thermoelectric properties of  $\text{Yb}_{0.15}\text{Co}_4\text{Sb}_{12}$  based nanocomposites with  $\text{CoSb}_3$  nano-inclusion. *Journal of Physics D: Applied Physics* **41**, 205403 (2008).
- [199] Pei, Y., Bai, S., Zhao, X., Zhang, W. & Chen, L. Thermoelectric properties of  $\text{Eu}_y\text{Co}_4\text{Sb}_{12}$  filled skutterudites. *Solid State Sciences* **10**, 1422–1428 (2008).
- [200] Qiu, P. F. *et al.* High-temperature electrical and thermal transport properties of fully filled skutterudites  $\text{RFe}_4\text{Sb}_{12}$  (R = Ca, Sr, Ba, La, Ce, Pr, Nd, Eu, and Yb). *Journal of Applied Physics* **109**, 063713 (2011).
- [201] Rogl, G., Grytsiv, A., Bauer, E., Rogl, P. & Zehetbauer, M. Thermoelectric properties of novel skutterudites with didymium:  $\text{DD}_y(\text{Fe}_{1-x}\text{Co}_x)_4\text{Sb}_{12}$  and  $\text{DD}_y(\text{Fe}_{1-x}\text{Ni}_x)_4\text{Sb}_{12}$ . *Intermetallics* **18**, 57–64 (2010).
- [202] Rogl, G., Grytsiv, A., Rogl, P., Bauer, E. & Zehetbauer, M. A new generation of *p*-type didymium skutterudites with high *ZT*. *Intermetallics* **19**, 546–555 (2011).
- [203] Rogl, G. *et al.* *n*-type skutterudites  $(\text{R,Ba,Yb})_y\text{Co}_4\text{Sb}_{12}$  (R = Sr, La, Mm, DD, SrMm, SrDD) approaching  $ZT \approx 2.0$ . *Acta Materialia* **63**, 30–43 (2014).
- [204] Rogl, G. *et al.* New bulk *p*-type skutterudites  $\text{DD}_{0.7}\text{Fe}_{2.7}\text{Co}_{1.3}\text{Sb}_{12-x}\text{X}_x$  (X = Ge, Sn) reaching  $ZT > 1.3$ . *Acta Materialia* **91**, 227–238 (2015).
- [205] Sales, B. C., Mandrus, D. & Williams, R. K. Filled skutterudite antimonides: A new class of thermoelectric materials. *Science* **272**, 1325–1328 (1996).
- [206] Shi, X. *et al.* Multiple-filled skutterudites: High thermoelectric figure of merit through separately optimizing electrical and thermal transports. *Journal of the American Chemical Society* **133**, 7837–7846 (2011).



- [207] Stiewe, C. *et al.* Nanostructured  $\text{Co}_{1-x}\text{Ni}_x(\text{Sb}_{1-y}\text{Te}_y)_3$  skutterudites: Theoretical modeling, synthesis and thermoelectric properties. *Journal of Applied Physics* **97**, 044317 (2005).
- [208] Su, X. *et al.* Structure and transport properties of double-doped  $\text{CoSb}_{2.75}\text{Ge}_{0.25-x}\text{Te}_x$  ( $x = 0.125-0.20$ ) with in situ nanostructure. *Chem. Mater.* **23**, 2948–2955 (2011).
- [209] Tang, X. F., Chen, L. D., Goto, T., Hirai, T. & Yuan, R. Z. Synthesis and thermoelectric properties of filled skutterudite compounds  $\text{Ce}_y\text{Fe}_x\text{Co}_{4-x}\text{Sb}_{12}$  by solid state reaction. *Journal of Materials Science* **36**, 5435–5439 (2001).
- [210] Xu, C., Duan, B., Ding, S., Zhai, P. & Zhang, Q. Thermoelectric properties of skutterudites  $\text{Co}_{4-x}\text{Ni}_x\text{Sb}_{11.9-y}\text{Te}_y\text{Se}_{0.1}$ . *Journal of Electronic Materials* **43**, 2224–2228 (2014).
- [211] Yang, K. *et al.* Synthesis and thermoelectric properties of double-filled skutterudites  $\text{Ce}_y\text{Yb}_{0.5-y}\text{Fe}_{1.5}\text{Co}_{2.5}\text{Sb}_{12}$ . *Journal of Alloys and Compounds* **467**, 528–532 (2009).
- [212] Zhang, X. *et al.* In situ synthesis and thermoelectric properties of  $(\text{Fe}/\text{Ni})_x\text{Co}_{4-x}\text{Sb}_{12}$  compounds by SPS. *Journal of Alloys and Compounds* **457**, 368–371 (2008).
- [213] Zhang, J. *et al.* High-pressure synthesis of phonon-glass electron-crystal featured thermoelectric  $\text{Li}_x\text{Co}_4\text{Sb}_{12}$ . *Acta Materialia* **60**, 1246–1251 (2012).
- [214] Zhao, W. *et al.* Enhanced thermoelectric performance in barium and indium double-filled skutterudite bulk materials via orbital hybridization induced by indium filler. *Journal of the American Chemical Society* **131**, 3713–3720 (2009).
- [215] Zhou, L., Qiu, P., Uher, C., Shi, X. & Chen, L. Thermoelectric properties of  $p$ -type  $\text{Yb}_x\text{La}_y\text{Fe}_{2.7}\text{Co}_{1.3}\text{Sb}_{12}$  double-filled skutterudites. *Intermetallics* **32**, 209–213 (2013).
- [216] Bali, A. *et al.* Thermoelectric properties of In and I doped PbTe. *Journal of Applied Physics* **120**, 175101 (2016).
- [217] Ding, G., Si, J., Yang, S., Wang, G. & Wu, H. High thermoelectric properties of  $n$ -type Cd-doped PbTe prepared by melt spinning. *Scripta Materialia* **122**, 1–4 (2016).
- [218] Jo, S. *et al.* Simultaneous improvement in electrical and thermal properties of interface-engineered BiSbTe nanostructured thermoelectric materials. *Journal of Alloys and Compounds* **689**, 899–907 (2016).
- [219] Joo, S.-J. *et al.* Thermoelectric properties of  $\text{Bi}_2\text{Te}_{2.7}\text{Se}_{0.3}$  nanocomposites embedded with MgO nanoparticles. *Journal of the Korean Physical Society* **69**, 1314–1320 (2016).
- [220] Li, Y. Y. *et al.* Enhanced thermoelectric performance of  $\text{Cu}_2\text{Se}/\text{Bi}_{0.4}\text{Sb}_{1.6}\text{Te}_3$  nanocomposites at elevated temperatures. *Appl. Phys. Lett.* **108**, 062104 (2016).
- [221] Li, Y., Liu, G., Qin, X. & Shan, F. Inhibition of minority transport for elevating the thermoelectric figure of merit of  $\text{CuO}/\text{BiSbTe}$  nanocomposites at high temperatures. *RSC Adv.* **6**, 112050–112056 (2016).
- [222] Liu, W. *et al.* Enhanced thermoelectric properties of  $n$ -type  $\text{Mg}_{2.16}(\text{Si}_{0.4}\text{Sn}_{0.6})_{1-y}\text{Sb}_y$  due to nano-sized Sn-rich precipitates and an optimized electron concentration. *Journal of Materials Chemistry* **22**, 13653 (2012).
- [223] Zhou, Y. M. *et al.* Strategy to optimize the overall thermoelectric properties of SnTe via compositing with its property-counter  $\text{CuInTe}_2$ . *Acta Materialia* **125**, 542–549 (2017).
- [224] Zhou, C. *et al.* Scalable solution-based synthesis of component-controllable ultrathin  $\text{PbTe}_{1-x}\text{Se}_x$  nanowires with high  $n$ -type thermoelectric performance. *J. Mater. Chem. A* **5**, 2876–2884 (2017).
- [225] Zhang, J. *et al.* Discovery of high-performance low-cost  $n$ -type  $\text{Mg}_3\text{Sb}_2$ -based thermoelectric materials with multi-valley conduction bands. *Nature Communications* **8**, 13901 (2017).
- [226] Xu, B. *et al.* Nanocomposites from solution-synthesized  $\text{PbTe}$ - $\text{BiSbTe}$  nanoheterostructure with unity figure of merit at low-medium temperatures (500–600 K). *Advanced Materials* **29**, 1605140 (2017).
- [227] Xie, D. *et al.* Stabilization of thermoelectric properties of the  $\text{Cu}/\text{Bi}_{0.48}\text{Sb}_{1.52}\text{Te}_3$  composite for advantageous power generation. *Journal of Electronic Materials* **46**, 2746–2751 (2017).
- [228] Wang, S. *et al.* High thermoelectric performance in Te-free  $(\text{Bi},\text{Sb})_2\text{Se}_3$  via structural transition induced band convergence and chemical bond softening. *Energy Environ. Sci.* **9**, 3436–3447 (2016).
- [229] Seo, S., Jeong, Y., Oh, M.-W. & Yoo, B. Effect of hydrogen annealing of ball-milled  $\text{Bi}_{0.5}\text{Sb}_{1.5}\text{Te}_3$  powders on thermoelectric properties. *Journal of Alloys and Compounds* **706**, 576–583 (2017).

- [230] Pei, Y. *et al.* Multiple converged conduction bands in  $\text{K}_2\text{Bi}_8\text{Se}_{13}$ : A promising thermoelectric material with extremely low thermal conductivity. *J. Am. Chem. Soc.* **138**, 16364–16371 (2016).
- [231] Park, K. *et al.* Extraordinary off-stoichiometric bismuth telluride for enhanced *n*-type thermoelectric power factor. *J. Am. Chem. Soc.* **138**, 14458–14468 (2016).
- [232] Moon, S. P. *et al.* Tunable thermoelectric transport properties of  $\text{Cu}_{0.008}\text{Bi}_2\text{Te}_{2.7}\text{Se}_{0.3}$  via control of the spark plasma sintering conditions. *Journal of the Korean Physical Society* **69**, 811–815 (2016).
- [233] Zhu, T. J., Cao, Y. Q., Yan, F. & Zhao, X. B. Nanostructuring and thermoelectric properties of semiconductor tellurides. In *Thermoelectrics, 2007. ICT 2007. 26th International Conference on*, 8–11 (IEEE, 2007).
- [234] Choi, J.-S. *et al.* Thermoelectric properties of *n*-type  $(\text{Pb}_{1-x}\text{Ge}_x)\text{Te}$  fabricated by hot pressing method. In *XVI International Conference on Thermoelectrics, 1997. Proceedings ICT '97*, 228–231 (1997).
- [235] Yamanaka, S., Kosuga, A. & Kurosaki, K. Thermoelectric properties of  $\text{Tl}_9\text{BiTe}_6$ . *Journal of Alloys and Compounds* **352**, 275–278 (2003).
- [236] Yang, S. H. *et al.* Nanostructures in high-performance  $(\text{GeTe})_x(\text{AgSbTe}_2)_{100-x}$  thermoelectric materials. *Nanotechnology* **19**, 245707 (2008).
- [237] Yang, S. H., Zhu, T. J., Zhang, S. N., Shen, J. J. & Zhao, X. B. Natural microstructure and thermoelectric performance of  $(\text{GeTe})_{80}(\text{Ag}_y\text{Sb}_{2-y}\text{Te}_{3-y})_{20}$ . *Journal of Electronic Materials* **39**, 2127–2131 (2010).
- [238] Zhang, S. N. *et al.* Effects of ball-milling atmosphere on the thermoelectric properties of TAGS-85 compounds. *Journal of Electronic Materials* **38**, 1142–1147 (2009).
- [239] Zhou, M., Li, J.-F. & Kita, T. Nanostructured  $\text{AgPb}_m\text{SbTe}_{m+2}$  system bulk materials with enhanced thermoelectric performance. *Journal of the American Chemical Society* **130**, 4527–4532 (2008).
- [240] Sharp, J. W. Some properties of GeTe-based thermoelectric alloys. In *Thermoelectrics, 2003 Twenty-Second International Conference on-ICT*, 267–270 (IEEE, 2003).
- [241] Salvador, J. R., Yang, J., Shi, X., Wang, H. & Wereszczak, A. Transport and mechanical property evaluation of  $(\text{AgSbTe})_{1-x}(\text{GeTe})_x$  ( $x=0.80, 0.82, 0.85, 0.87, 0.90$ ). *Journal of Solid State Chemistry* **182**, 2088–2095 (2009).
- [242] Levin, E. M. *et al.* Analysis of Ce- and Yb-Doped TAGS-85 materials with enhanced thermoelectric figure of merit. *Advanced Functional Materials* **21**, 441–447 (2011).
- [243] Yamanaka, S., Kobayashi, H. & Kurosaki, K. Thermoelectric properties of layered rare earth copper oxides. *Journal of alloys and compounds* **349**, 321–324 (2003).
- [244] Zhao, L.-D. *et al.* Thermoelectric and mechanical properties of nano-SiC-dispersed  $\text{Bi}_2\text{Te}_3$  fabricated by mechanical alloying and spark plasma sintering. *Journal of Alloys and Compounds* **455**, 259–264 (2008).
- [245] Zhao, X. Y. *et al.* Synthesis and thermoelectric properties of Sr-filled skutterudite  $\text{Sr}_y\text{Co}_4\text{Sb}_{12}$ . *Journal of Applied Physics* **99**, 053711 (2006).
- [246] Yu, C. *et al.* High-performance half-Heusler thermoelectric materials  $\text{Hf}_{1-x}\text{Zr}_x\text{NiSn}_{1-y}\text{Sb}_y$  prepared by levitation melting and spark plasma sintering. *Acta Materialia* **57**, 2757–2764 (2009).
- [247] Xiong, Z., Chen, X., Huang, X., Bai, S. & Chen, L. High thermoelectric performance of  $\text{Yb}_{0.26}\text{Co}_4\text{Sb}_{12}/y\text{GaSb}$  nanocomposites originating from scattering electrons of low energy. *Acta Materialia* **58**, 3995–4002 (2010).
- [248] Toberer, E. S. *et al.* Traversing the metal-insulator transition in a Zintl phase: Rational enhancement of thermoelectric efficiency in  $\text{Yb}_{14}\text{Mn}_{1-x}\text{Al}_x\text{Sb}_{11}$ . *Advanced Functional Materials* **18**, 2795–2800 (2008).
- [249] Chung, D.-Y. *et al.*  $\text{CsBi}_4\text{Te}_6$ : A high-performance thermoelectric material for low-temperature applications. *Science* **287**, 1024–1027 (2000).
- [250] Tang, X., Li, P., Deng, S. & Zhang, Q. High temperature thermoelectric transport properties of double-atom-filled clathrate compounds  $\text{Yb}_x\text{Ba}_{8-x}\text{Ga}_{16}\text{Ge}_{30}$ . *Journal of Applied Physics* **104**, 013706 (2008).

- [251] Mi, J. L., Zhao, X. B., Zhu, T. J. & Tu, J. P. Improved thermoelectric figure of merit in  $n$ -type  $\text{CoSb}_3$  based nanocomposites. *Applied Physics Letters* **91**, 172116 (2007).
- [252] Liu, W.-S., Zhang, B.-P., Zhao, L.-D. & Li, J.-F. Improvement of thermoelectric performance of  $\text{CoSb}_{3-x}\text{Te}_x$  skutterudite compounds by additional substitution of IVB-group elements for Sb. *Chemistry of Materials* **20**, 7526–7531 (2008).
- [253] Li, H., Tang, X., Su, X. & Zhang, Q. Preparation and thermoelectric properties of high-performance Sb additional  $\text{Yb}_{0.2}\text{Co}_4\text{Sb}_{12+y}$  bulk materials with nanostructure. *Applied Physics Letters* **92**, 202114 (2008).
- [254] Chen, L. D., Huang, X. Y., Zhou, M., Shi, X. & Zhang, W. B. The high temperature thermoelectric performances of  $\text{Zr}_{0.5}\text{Hf}_{0.5}\text{Ni}_{0.8}\text{Pd}_{0.2}\text{Sn}_{0.99}\text{Sb}_{0.01}$  alloy with nanophase inclusions. *Journal of Applied Physics* **99**, 064305 (2006).
- [255] Zhong, B. *et al.* High superionic conduction arising from aligned large lamellae and large figure of merit in bulk  $\text{Cu}_{1.94}\text{Al}_{0.02}\text{Se}$ . *Applied Physics Letters* **105**, 123902 (2014).
- [256] Yu, B. *et al.* Thermoelectric properties of copper selenide with ordered selenium layer and disordered copper layer. *Nano Energy* **1**, 472–478 (2012).
- [257] Liu, H. *et al.* Ultrahigh thermoelectric performance by electron and phonon critical scattering in  $\text{Cu}_2\text{Se}_{1-x}\text{I}_x$ . *Advanced Materials* **25**, 6607–6612 (2013).
- [258] Liu, H. *et al.* Copper ion liquid-like thermoelectrics. *Nature Materials* **11**, 422–425 (2012).
- [259] He, Y., Zhang, T., Shi, X., Wei, S.-H. & Chen, L. High thermoelectric performance in copper telluride. *NPG Asia Mater* **7**, e210 (2015).
- [260] Gahtori, B. *et al.* Giant enhancement in thermoelectric performance of copper selenide by incorporation of different nanoscale dimensional defect features. *Nano Energy* **13**, 36–46 (2015).
- [261] Day, T. W. *et al.* High-temperature thermoelectric properties of  $\text{Cu}_{1.97}\text{Ag}_{0.03}\text{Se}_{1+y}$ . *Materials for Renewable and Sustainable Energy* **3** (2014).
- [262] Ballikaya, S., Chi, H., Salvador, J. R. & Uher, C. Thermoelectric properties of Ag-doped  $\text{Cu}_2\text{Se}$  and  $\text{Cu}_2\text{Te}$ . *J. Mater. Chem. A* **1**, 12478–12484 (2013).
- [263] Bailey, T. P. *et al.* Enhanced  $ZT$  and attempts to chemically stabilize  $\text{Cu}_2\text{Se}$  via Sn doping. *J. Mater. Chem. A* **4**, 17225–17235 (2016).
- [264] Li, W. *et al.* Promoting  $\text{SnTe}$  as an eco-friendly solution for  $p$ - $\text{PbTe}$  thermoelectric via band convergence and interstitial defects. *Advanced Materials* **29**, 1605887 (2017).
- [265] Plot Digitizer description. <http://plotdigitizer.sourceforge.net/>. Accessed: 2018-10-05.
- [266] Chung, J. & Ryu, B. Nonlocal problems arising in thermoelectrics. *Mathematical Problems in Engineering* **2014**, 1–7 (2014).
- [267] Goupil, C. *Continuum theory and modeling of thermoelectric elements* (John Wiley & Sons, 2015).
- [268] Burden, R. L. & Faires, J. D. *Numerical analysis* (Brooks/Cole, Cengage Learning, 2010), 9th edn.
- [269] Kim, H. S., Liu, W., Chen, G., Chu, C.-W. & Ren, Z. Relationship between thermoelectric figure of merit and energy conversion efficiency. *Proceedings of the National Academy of Sciences* **112**, 8205–8210 (2015).
- [270] Hohenberg, P. & Kohn, W. Inhomogeneous electron gas. *Physical review* **136**, B864 (1964).
- [271] Kohn, W. & Sham, L. J. Self-consistent equations including exchange and correlation effects. *Physical review* **140**, A1133 (1965).
- [272] Perdew, J. P., Burke, K. & Ernzerhof, M. Generalized gradient approximation made simple. *Physical review letters* **77**, 3865 (1996).
- [273] Blöchl, P. E. Projector augmented-wave method. *Physical review B* **50**, 17953 (1994).
- [274] Kresse, G. & Furthmüller, J. Efficient iterative schemes for *ab initio* total-energy calculations using a plane-wave basis set. *Phys. Rev. B* **54**, 11169 (1996).
- [275] Kresse, G. & Joubert, D. From ultrasoft pseudopotentials to the projector augmented-wave method. *Physical Review B* **59**, 1758 (1999).
- [276] Madsen, G. K. & Singh, D. J. Boltztrap. A code for calculating band-structure dependent quantities. *Computer Physics Communications* **175**, 67–71 (2006).

- [277] Ryu, B., Chung, J., Choi, E.-A., Kim, B.-S. & Park, S.-D. Thermoelectric power factor of Bi-Sb-Te and Bi-Te-Se alloys and doping strategy: First-principles study. *Journal of Alloys and Compounds* **727**, 1067–1075 (2017).
- [278] Togo, A., Chaput, L. & Tanaka, I. Distributions of phonon lifetimes in brillouin zones. *Phys. Rev. B* **91**, 094306 (2015).
- [279] Ryu, B. & Oh, M.-W. Computational simulations of thermoelectric transport properties. *Journal of the Korean Ceramic Society* **53**, 273–281 (2016).